Mitochondrial phenotypes in purified human immune cell subtypes and cell mixtures

Shannon Rausser[1], Caroline Trumpff[1], Marlon A McGill[1], Alex Junker[1], Wei Wang[2], Siu-hong Ho[2], Anika Mitchell[1], Kalpita R Karan[1], Catherine Monk[1,5,6], Suzanne C. Segerstrom[3], Rebecca G. Reed[4], Martin Picard[1,6,7]

[1] Department of Psychiatry, Division of Behavioral Medicine, Columbia University Irving Medical Center, New York, NY 10032, USA

[2] Columbia Center for Translational Immunology, Columbia University Irving Medical Center, New York, NY 10032, USA

[3] Department of Psychology, University of Kentucky, Lexington, KY, 40506, USA

[4] Department of Psychology, University of Pittsburgh, Pittsburgh, PA, 15260, USA

[5] Department of Neurology, Merritt Center, Columbia University Irving Medical Center, New York, NY 10032, USA

[6] Department of Obstetrics & Gynecology, Columbia University Irving Medical Center, New York, NY 10032, USA

[7] New York State Psychiatric Institute, New York, NY 10032, USA

Correspondence: martin.picard@columbia.edu

Abstract

Mitochondrial function studies in human leukocytes have mainly focused on peripheral blood mononuclear cells (PBMCs), with the assumption that the immunometabolic properties of different immune cells have a negligible effect on PBMCs. Using a high-throughput mitochondrial phenotyping platform to quantify multiple mitochondrial features among both PBMCs and immunologically-defined immune cell subtypes from the same individuals, we show how mitochondrial activity in PBMCs is confounded by both cell type distributions and contaminating platelets. Then, applying this cell-specific approach in women and men spanning 4 decades of life, we find that mitochondria exhibit specific age- and sex-related differences, including an age-related elevation in mitochondrial DNA copy number (mtDNAcn), which are masked or blunted in PBMCs. Our purified cell subtypes data also define in humans the variation in mtDNAcn, mitochondrial content (citrate synthase), and respiratory chain enzymatic activities among neutrophils, monocytes, B and T lymphocyte subtypes. Moreover, we validate these cell type differences and define the natural intra-individual variation in mitochondrial function using an intensive repeated-measures study in a single individual, revealing substantial natural variation over time among cell subtypes and PBMCs. Finally, we introduce multivariate mitochondrial phenotypes – *mitotypes* – that distinguish lymphoid from myeloid cell types, naïve-to-memory lymphocyte states, and moderately differ between women and men, which we propose as potential cell-specific biomarkers for future studies. Together, these findings identify dynamic cell-type specific variation in mitochondrial biology in circulating human leukocytes, providing foundational knowledge to develop interpretable blood-based assays of mitochondrial health.

Keywords: mitochondria; leukocytes; sexual dimorphism; aging; dynamic variation

Introduction

Mitochondria are the most studied organelle across biomedical sciences[1]. Accumulating evidence implicate mitochondrial (dys)function as a major determinant of disease risk and aging[1, 2, 3] and as a mediator of psycho-biological processes[4]. As a consequence, there is an increasing interest to develop tractable biomarkers and quantify mitochondrial content (the mass of mitochondria per cell) and function (energy production capacity) in accessible human tissues, such as peripheral blood leukocytes. Although some research has applied cell-specific assays to interrogate mitochondrial function in immune cells[5], the majority of studies have examined peripheral blood mononuclear cells (PBMCs), with the assumption that the immunometabolic properties of different immune cells have a negligible effect on PBMCs. However, it remains unclear to what extent mitochondrial measurements in PBMCs are confounded by biological factors such as: i) cell type composition, ii) platelet contamination, iii) mitochondrial properties across different immune cells, and iv) the variability of cell type composition and bioenergetics over time. These four main gaps in knowledge limit rational decision making about the need to collect purified cell populations to reliably quantify mitochondrial function in observational and intervention studies.

As part of normal human physiology, specific immune cell types are mobilized from lymphoid organs into circulation in a diurnal fashion, substantially influencing the pool of peripheral blood leukocyte composition[6]. Moreover, the circulating abundance of immune cell subtypes is highly variable between individuals, a feature partially attributable to both individual-level (e.g., sex and age) and environmental factors[7]. So PBMCs from different individuals reflect different cell populations. This is significant since the major immune cell types differ in their respiratory properties and mitochondrial RC protein abundance[5, 8, 9], with mixed lymphocytes and monocytes exhibiting substantial differences[10]. Therefore, we hypothesized that the relative abundance of different cell types (i.e., cell type composition) confounds measurements of mitochondrial functions in PBMCs. Furthermore, commonly used Ficoll-isolated PBMCs are contaminated with (sticky) platelets, which themselves contain mitochondria and mtDNA but no nuclear genome to use as reference for mtDNA copy number (mtDNAcn) measurements[11]. This adds another potential source of bias to mitochondrial studies in PBMCs or other undefined cell mixtures[12, 13, 14]. To enable scalable translational mitochondrial research, there is therefore a need to develop biologically valid measures of mitochondrial health in specific immune cells and to quantify the influence of cell type abundance and platelet contamination on specific features of mitochondrial behavior beyond mtDNAcn.

Mitochondria are multifunctional organelles that are not all created equal – various features of mitochondrial content and function vary based on the tissue and cell type they inhabit[15, 16] a phenomenon termed functional specialization[17]. But little is known about the nature and magnitude of inter-individual differences in mitochondrial phenotypes within specific molecularly-defined immune cell subtypes. The immune system provides a particularly powerful system to examine this question since the acquisition of specialized cellular characteristics during differentiation is known to be determined by changes in mitochondrial metabolism[18]. For example, the activation, proliferation, and differentiation of both monocytes[19] and T cells[20] into specific effector cells require distinct metabolic profiles and cannot proceed without the proper metabolic states. Likewise, naïve and memory T lymphocytes differ in their reliance on mitochondrial oxidative phosphorylation (OXPHOS) involving the respiratory chain (RC) enzymes[21, 22, 23], and harbor differences in protein composition and mitochondrial content within the cytoplasm[24]. Thus, we hypothesized that circulating immune cell subtypes in human blood should exhibit robust differences in mitochondrial phenotypes (mitotypes) including both features of mitochondrial content and RC function.

An equally significant gap in knowledge relates to the natural dynamic variation in mitochondrial content and function. Mitochondria dynamically recalibrate in response to stress exposure (for a review see[25]), and well-defined mitochondrial recalibrations to stress[25] and exercise[26] suggest that cell-specific mitochondrial features could exhibit natural variation over time. Are leukocyte mitochondrial content and RC function stable trait-like properties of each person, or are they state-like features that vary over time, possibly in response to metabolic or endocrine mediators?

To address these questions, we deployed a high-throughput mitochondrial phenotyping platform on immunologically-defined immune cell subtypes, in parallel with PBMCs, to define cell-specific, multivariate mitochondrial phenotypes[27]. First, we establish the extent to which cell type composition and platelet contamination influence PBMCs-based mitochondrial measures. We then systematically map the mitochondrial properties of different immune cell subtypes, and validate the existence of stable mitochondrial phenotypes in an intensive repeated-measures design within the same individual, which also reveals a surprising degree of change over time. Collectively, these data (1) highlight the inadequacy of PBMCs to profile human mitochondrial function between individuals and over time, and (2) define unique cell-specific mitochondrial features in circulating human leukocytes in relation to age, sex, and biomarkers. These data

represent a resource to design cell-specific immune mitochondrial phenotyping strategies in future studies.

Results

Cell subtype distributions by age and sex

Our goal was to perform mitochondrial profiling on molecularly-defined subtypes of immune cell populations in parallel with PBMCs collected at the same time. Twenty one participants (11 women, 10 men) distributed across 4 decades of life (ages 20-59, 4-8 participants per decade across both sexes) were recruited, and ~100ml of blood was collected; total leukocytes were then labeled with two cell surface marker cocktails, counted and isolated by fluorescence-activated cell sorting (FACS, see *Methods* for details), and processed on our mitochondrial phenotyping platform adapted from [27] (Figure 1a). In parallel, a complete blood count (CBC) for the major leukocyte populations in whole blood, standard blood chemistry, and a metabolic and endocrine panel were assessed (Figure 1b).

We first quantified the abundance of specific cell subtypes based on cell surface marker combinations listed in Figure 1c (see Supplemental Figures 1 and 2 for the gating strategy, and Supplemental Table 1), including innate (neutrophils, NK cells, and monocytes) and adaptive T and B lymphocytes. We further distinguished $CD4^+$ and $CD8^+$ T cells by their naïve and memory states, including central (CM) and effector memory (EM), as well as terminally differentiated effector memory cells re-expressing CD45RA (TEMRA) subtypes. Evaluating the abundance of each cell subtype among participants, we found that compared to women, men had on average 35-44% more NK cells and monocytes, but 66% fewer $CD4^+$ naïve T cells (Figure 1d). These differences were characterized by moderate to large standardized effect sizes (Hedges' g=0.71-0.93), confirming as previously established[7] that the composition of circulating immune cells differ between women and men. Even between individual participants of the same sex, the circulating proportions of various cell subtypes (e.g., B and T lymphocytes, monocytes) varied by up to an order of magnitude (i.e., 10-fold) (Figure 1e).

In relation to age, as expected[7] $CD8^+$ naïve T cells abundance was lower in older individuals ($p<0.01$). Specifically, compared to young adults in their 20's, middle-aged individuals in their 50's had on average ~63% fewer $CD8^+$ naïve T cells (Figure 1f). In contrast, $CD4^+$ EM and $CD8^+$ CM abundance tended to increase with age (positive correlation, r=0.31 for both), an overall picture consistent with immunological aging[7, 28].

CBC-derived cell proportions also showed that compared to women, men had on average 28% more monocytes (Supplemental Figure 3), consistent with our FACS results. Conversely, compared to men, women had on average 20% more platelets. Platelet abundance also tended to decrease with age, a point discussed later.

Next, we built on these results to examine the influence of blood cell type composition and platelets on mitochondria in PBMCs. Our analysis focused on two broad aspects of mitochondrial biology: i) *mitochondrial content*, indexed by citrate synthase (CS) activity, a Kreb's cycle enzyme used as a marker of mitochondrial volume density[29], and mtDNAcn, reflecting the number of mtDNA copies per cell; and ii) *RC function* measured by complex I (CI), complex II (CII) and complex IV (CIV) enzymatic activities, which reflect the capacity for electron transport and respiratory capacity and serve here as a proxy for maximal oxidative phosphorylation (OXPHOS) capacity (Figure 1a). Furthermore, by adding the three mean-centered features of RC function together as a numerator (CI+CII+CIV), and dividing this by the combination of content features (CS+mtDNAcn), we obtained an index reflecting *RC capacity on a per-mitochondrion basis*, known as the mitochondrial health index (MHI) adapted from previous work[27].

Circulating cell composition influence mitochondrial features in PBMCs

Compared to isolating purified cell subtypes, cell mixtures such as PBMCs are more easily collected and require less blood volume to obtain a sufficient number of cells for downstream analyses. As a result, PBMCs have been the preferred material of choice in human leukocyte studies examining environmental influences on mitochondria (e.g., [27, 30, 31, 32, 33, 34]). However, in light of i) large variation in the abundance of circulating cell types, both between- and within-person, and ii) general bioenergetic differences between the major cell types[5], we hypothesize that cell mixtures are likely to be confounded by cell type distribution.

We first established how much the abundance of various circulating immune cell subtypes correlates with individual mitochondrial metrics in PBMCs. The null hypothesis was that cell type abundances (e.g., having more or fewer B cells in circulation) does not influence PBMCs mitochondrial features. The proportion of variance in PBMCs mitochondrial features attributable to cell type abundance measured by flow cytometry is shown in Figure 2a. Contrary to the null hypothesis, the abundance of multiple circulating cells correlated with PBMCs mitochondrial features. Notably, the proportion of circulating B cells accounted for 27% of the variance (r^2) in PBMCs mtDNAcn, and for 32-61% of the variance in CS, CI, and CII activities. These findings were consistent with the fact that individuals varied substantially in B cell proportions (range:

<0.01-15.3%) (Supplemental Table 2), and that B cells exhibited the highest mtDNAcn of all cell subtypes (see below). The proportion of other cell types accounted for more modest portions (<14%) of the variance in PBMCs, although we note that higher abundance of memory cells tended to be negatively associated with PBMCs RC enzymatic activities.

This analysis was repeated with CBC-derived cell proportions to examine the association of broad leukocyte groups with mitochondrial features in PBMCs. The abundance of eosinophils and neutrophils was positively correlated with most PBMCs mitochondrial content and activity features (Supplemental Figure 4a). Because PBMCs do not contain granulocytes, it appears more likely that these correlations reflect the independent effect of a humoral factor on cell mobilization and mitochondrial function.

Together, these data demonstrate that mitochondrial features assessed in PBMCs in part reflect the proportions of some but not all circulating cell subtypes. Therefore, these results objectively document cell type distribution as a major confounding factor in the measurements of mitochondrial function in PBMCs.

Platelets influence PBMCs mitochondrial phenotypes

Platelets contain mitochondria and mtDNA, but no nucleus. Because cell-based qPCR-based procedures rely on the presence of the nuclear genome to quantify mtDNA copies per cell, platelets are essentially invisible to cell-based normalization procedures and therefore inflate mitochondrial activities on a per-cell basis[12, 13]. Moreover, platelets are naturally adherent and easily form platelet-leukocyte aggregates[35], such that they typically “contaminate” leukocyte preparations and inflate mtDNAcn measurements[11, 12, 13, 14] (Figure 3a). Therefore, to partly resolve the origin of the discrepancies between isolated cell subtypes and PBMCs noted above, we sought to directly quantify the contribution of platelets to total mitochondrial content and activity features in PBMCs. We note that the PBMCs used in our study were carefully prepared with two passive platelet depletion steps consisting of low centrifugation spins where leukocytes sediment but platelets float (see Methods for details). Thus, theoretically, our PBMCs should be “platelet-free”.

We first asked if the abundance of platelets from the CBC data in the cohort varies by age. In our cohort, we found that platelet count decreased by 6% for each decade of life (Figure 3b), declining by an average of 24% between the ages of 20 and 60. The loss of platelets with age, in women and men, is consistent with two large epidemiological studies of >40,000 individuals each[36, 37], although the effect sizes vary by cohort and our estimate is likely overestimated due to

the small sample size (Figure 3c). As expected, we also found that total blood platelet count tended to be consistently *positively* correlated with mtDNAcn, CS and RC activities in PBMCs (r=0.031-0.38) (Figure 3d), suggesting that PBMCs preparations from individuals with more circulating platelets may also contain more contaminating platelets. Therefore, the age-related loss of platelets and of the mtDNA contained within them could account for the previously reported age-related decline in mtDNAcn from studies using either whole blood[38, 39] (which includes all platelets) or PBMCs[40] (which includes fewer contaminating platelets).

To directly test this hypothesis, we ran a separate experiment to quantify the influence of platelets on multiple mitochondrial features in PBMCs (Figure 3e). This consisted of isolating PBMCs using standard methods, which again included two commonly-used low speed "platelet depletion" steps (see *Methods* for details). A portion of the obtained PBMCs platelets were then actively immunodepleted using anti-CD61-tagged magnetic beads. Three fractions were ultimately processed for mitochondrial phenotyping and compared: i) total PBMCs, ii) active platelet-depleted PBMCs, and iii) platelet-enriched eluate from the depletion procedure. As expected, platelet depletion decreased mtDNAcn, CS, and RC activities, indicating that contaminating platelets exaggerated specific mitochondrial features by 9-22%, with the exception of complex IV (Figure 3f). Moreover, the platelet-enriched eluate showed 23-100% higher mitochondrial activities relative to total PBMCs, providing further evidence that platelet depletion was effective and that platelets inflate estimates of mitochondrial abundance and RC activity in standard PBMCs.

Interestingly, the composite MHI was not affected by the platelet depletion procedure, suggesting that this multivariate index of respiratory chain capacity on a per-mitochondrion basis may be more robust to platelet contamination than its individual features. Overall, these data demonstrate platelet-contamination even in carefully prepared PBMCs, and show that the magnitude of platelet contamination significantly alters specific mitochondrial metrics in PBMCs-based mitochondrial studies.

Individual cell subtypes are biologically distinct from PBMCs

Having established that PBMCs provide an imperfect picture of mitochondrial function implies that specific leukocyte cell subtypes should be studied. To address these questions, we next deployed our mitochondrial phenotyping platform in both FACS-purified immune cells and PBMCs collected simultaneously to define their unique properties. To obtain sufficient numbers of cells for mitochondrial phenotyping, we selected the 6 most abundant cell subtypes for each

individual and isolated 5 million cells for each sample. Because memory subtypes were relatively rare, central and effector memory (CM and EM) subtypes were pooled for $CD4^+$ and/or $CD8^+$ (CM-EM). This generated a total of 340 biological samples, including 136 biological replicates, yielding 204 individual person-to-cell-type combinations used for mitochondrial phenotyping.

If PBMCs were comprised solely of those individual cell types, mitochondrial activities normalized on a per-cell basis in PBMCs could only be as high as the highest cell subtype it contains (e.g., B cells), and as low as the lowest (e.g., neutrophils). Curiously, we found that PBMCs had up to 2.9-fold higher levels of CS, CI, and CII activity per cell than any of the individual cell subtypes measured (see Figure 4), casting initial doubt on the validity of mitochondrial activity measures in PBMCs. This discrepancy could in part be attributable to contamination of PBMCs with platelets, or by the presence of other (unknown) cell types.

Among cell subtypes, CS activity was highest in monocytes and B cells, and lowest in $CD4^+$ naïve T cells, with other cell types exhibiting intermediate levels (Figure 4a). Regarding mitochondrial genome content, B cells had the highest mtDNAcn with an average 451 copies per cell compared to neutrophils and NK cells, which contained only an average of 128 ($g=5.94$, $p<0.0001$) and 205 copies ($g=3.84$, $p<0.0001$) per cell, respectively (Figure 4b). The low mtDNAcn in neutrophils relative to lymphocytes is in line with previous research[8, 9]. Naïve and memory $CD4^+$ and $CD8^+$ T lymphocytes had intermediate mtDNAcn levels of ~300 copies per cell, with the exception of $CD8^+$ naïve cells (average of 427 copies per cell). Between cell types, we note that CS activity and mtDNAcn differed by up to 3.52-fold, providing initial evidence of strong effect size segregation of cell type-specific mitochondrial phenotypes among both innate and adaptive cell lineages.

In relation to RC function, monocytes had the highest Complexes I, II, and IV activities. Consistent with their low mtDNAcn, neutrophils also had the lowest activities across complexes, whereas naïve and memory subtypes of T and B lymphocytes presented intermediate RC enzyme activities (Figure 4c-e).

To understand the proportion of shared variance between mitochondrial content features (CS and mtDNA) and between RC complex enzymatic activities, we quantified their inter-correlations among all cell types. Consistent with previous work in PBMCs[27], CS activity and mtDNAcn were positively correlated with each other, as were RC complexes CI, CII, and CIV (Figure 4f). Interestingly among cell subtypes, CS and mtDNAcn were only weakly correlated with each other, and in some cases were negatively correlated. For RC complexes CI, CII, and CIV,

which physically interact and whose function is synergistic within the inner mitochondrial membrane, correlations tended to be positive, as expected (Figure 4f). However, some of these correlations were weak, and some were either not correlated or even negatively correlated within specific cell types. These relatively weak and absent inter-correlations between mitochondrial features in some cell types reveal that each metric (i.e., content features and enzymatic activities) provides relatively independent, rather than redundant, information about the immune cell mitochondrial phenotype. Moreover, we note that PBMCs consistently showed the highest inter-correlations among mitochondrial features (above all cell types), which is consistent with the amalgamation or "homogenization" of cell-specific features.

Mitochondrial health index (MHI) among cell subtypes

We use the composite MHI to further define how RC function relates to mitochondrial content (Figure 5a). There was a significant difference in MHI between cell types ($p<0.0001$). Of all cell types, monocytes had the highest MHI, which was 72% higher than B cells ($g=3.78$, $p<0.0001$) which had the lowest MHI (Figure 5b). On average, memory T cell subtypes exhibited a 6-18% higher MHI relative to their naïve precursors ($CD4^+$: $g=0.40$, $p=0.32$; $CD8^+$: $g=1.02$, $p=0.019$), consistent with the notion that naïve and activated immune cells have different bioenergetic requirements[41, 42]. The PBMCs MHI was intermediate between values of monocytes and lymphocytes.

Mitochondrial features exhibit differential co-regulation across immune cell subtypes

We next asked to what extent mitochondrial markers are correlated among different cell subtypes in the same person. For example, does the individual with the highest mtDNAcn in B cells also have the highest mtDNAcn in other cell types? Could having high mtDNAcn or low MHI activity constitute coherent properties of an individual that are expressed ubiquitously across cell types, or are these properties specific to each cell subtype?

To assess the extent to which mitochondrial features are correlated across cell subtypes (co-regulation), we generated Spearman correlation matrices, which revealed a general positive association (Figure 5c). Within a person, CS activity was moderately co-regulated across cell subtypes (average correlation $r_{z'}=0.63$), albeit with some exceptions (i.e., cell pairs that were less correlated than average, such as $CD4^+$ CM-EM T cells & B cells). Similarly, mtDNAcn was generally positively correlated between cell types (average correlation $r_{z'}=0.53$). We note that compared to CM-EM subtypes, naïve T lymphocyte mtDNAcn values tended to be more strongly correlated with other cell subtypes ($r=0.32$-0.93), indicating that co-regulation of mtDNAcn differs

between cell types. In comparison, RC enzymes showed markedly lower inter-correlations across cell types (Figure 5d) and some cell types showed no correlation with other cell types, revealing a substantially lower degree of co-regulation among RC components than in mitochondrial content features. However, there was moderate and consistent positive co-regulation across cell types for MHI (average $r_{z'}$=0.37). PBMCs exhibited moderate to no correlation with other cell subtypes (Figure 5c, Supplemental Figure 4a), further indicating their departure from purified subtypes.

Together, these findings show that while immune cells exhibit markedly different mitochondrial content and RC activities (see Figure 4), there is consistent evidence for a person-level factor. On the other hand, the absence of correlation among several cell types, particularly for RC enzymatic activities, suggests that the biology of immune cell subtypes could be relatively independently determined by cell-autonomous factors (e.g., stimulation of specific cell subtypes or subpopulations). These subtype-resolution results therefore provide a strong rationale for performing cell-type specific studies when examining the influence of external exposures and person-level factors on immune cells' mitochondrial bioenergetics, including the influence of sex and age.

Mitochondrial content and RC function differ between women and men

To evaluate the added value of cell subtype specific studies when applied to real-world questions, we then systematically compared CS activity, mtDNAcn, RC activity, and MHI between women and men, asking to what extent the influence of sex on mitochondrial phenotypes can be detected in purified cell subtypes and PBMCs. Across all cell subtypes examined, compared to men, women had higher CS activity (range: 4-29%, g=0.20-1.52, Figure 6a) and higher CII activity (range:1-10%, g=0.03-0.56, Figure 6d). The consistency of this finding across *all* cell types suggests that these differences are stable, sexually dimorphic characteristics. Women also showed 29% higher CS activity in $CD8^+$ memory subsets and 26% higher CI activity in monocytes, differences that were characterized by strong effect sizes (g=1.52 and 1.35, respectively, Figure 6a and c).

Compared to women, men exhibited higher mtDNAcn in monocytes and neutrophils (range: 5-12%, g=0.37-0.73, Figure 6b), higher CI activity in neutrophils and NK cells (range: 9-13%, g=0.26-0.64, Figure 4c), and higher CIV activity specifically in B cells (20%, g=0.53, Figure 6e). Cells exhibiting the largest degree of sexual dimorphism on the integrated MHI were neutrophils (17% higher in women, g=0.52) and B cells (12% higher in men, g=0.73) (Figure 6f).

In contrast, none of these differences were detectable in PBMCs, illustrating the limitation of mixed cells to examine sex differences in mitochondrial function. These data reveal cell subtype-specific (and possibly lineage-specific) sex differences in human immune cell mitochondria.

Age influences mitochondrial content and RC function

We then quantified the association between the same mitochondrial features and age as correlations for each cell subtype, and in PBMCs. With increasing age, CS activity was relatively unaffected except in neutrophils, where it decreased ~7% per decade (r=-0.63, p=0.031) (Figure 6g). In comparison, mtDNAcn increased with increasing age among all cell subtypes except $CD8^+$ naïve T cells. Interestingly, $CD8^+$ naïve T cells were the cell subtype exhibiting the strongest age-related decline in circulatory abundance. $CD4^+$ naïve T cells and monocytes showed the largest age-related change in mtDNAcn, marked by a ~10% increase in the number of mitochondrial genome copies per cell per decade of life (r=0.54 for both, p=0.022 and 0.023 respectively, Figure 6h). The age-related increase in mtDNAcn in $CD4^+$ T cells is consistent with the increase in mitochondrial respiratory chain proteins in this cell population[24]. Thus, in specific cell subtype preparations, aging is associated with a consistent increase in leukocyte mtDNAcn.

For RC function, we observed an equal number of cell subtypes with either positive or negative correlations with age, with the exception of CII (Figures 6i-k). CII activity was positively correlated with age across all cell types, except for monocytes and NK cells where it was independent from age. In contrast, CI and CIV activities were only weakly associated with age, highlighting again differential regulation and partial “biological independence" of different RC components. Of all cell types, $CD8^+$ CM-EM T cells showed the most consistent positive associations for all RC activities and age, most notably for CII where the enzymatic activity per cell increased a striking ~21% per decade (r=0.85, p=0.0004). $CD4^+$ naïve T cells were the only cell type showing a consistent, albeit modest, increase of both mitochondrial content and function with age (range:1-10% increase per decade, r=0.08-0.54, Supplemental Figure 5). Similarly, MHI correlated positively with age in $CD8^+$ CM-EM T cells, indicating that energy production capacity on a per-mitochondrion basis tends to increase with age in this cell type (r=0.56, p=0.052), possibly related to the acquisition or maintenance of memory characteristics. In contrast, MHI tended to correlate negatively with age in monocytes (r=-0.35, p=0.15) (Figure 6l).

Overall, these data demonstrate that age-related changes in CS activity, mtDNAcn, and RC function are largely cell-type specific. This conclusion is further reinforced by analyses of PBMCs where mitochondrial features consistently did not significantly correlate with age (r=0.008-

0.15, absolute values) (Figure 4g-l). Thus, PBMCs appear insensitive to robust cell-type specific mitochondrial recalibrations with age, again highlighting the value of cell-specific measurements.

Cell subtype distributions exhibit natural week-to-week variation

Whether and how much mitochondrial content/function change over time is not well defined, and to our knowledge has not been examined in circulating human immune cells. To examine this question, we repeated the same blood collection, cell sorting, and downstream mitochondrial enzymatic and molecular profiling described above on a healthy 34-year-old Caucasian man (author M.P.), weekly over 9 weeks (Figure 7a). To preclude external influences of cell subtype distributions and mitochondrial function, each blood draw occurred at the same time of the day (9:00-9:30am), on the same day of the week, after a standardized breakfast and comparable physical activity. The 6 most abundant cell subtypes for this individual included: neutrophils, NK cells, monocytes, naïve and CM-EM subtypes of $CD4^+$ T cells, and naïve $CD8^+$ T cells. The resulting samples were processed on the mitochondrial phenotyping platform in parallel with the cohort samples, ensuring that results across the cohort and repeat participant are directly comparable.

We first quantified the circulating proportions (% of total leukocytes by FACS) of 12 cell types to establish how much the abundance of each cell subtype naturally varies within a person (Supplemental Figure 6). Cell type distribution is known to exhibit natural diurnal variation[6, 43] and can be altered with stress exposure in rats and humans[44, 45]. The cell subtype with the least week-to-week variation in abundance was $CD8^+$ EM (root mean square of successive differences [rMSSD]=0.22, coefficient of variation [C.V.]=19.5%), which varied between 6.3% (week 2, highest) to 3.3% of total cells (week 9, lowest). Thus, even the least variable cell type can decrease/increase in proportion by approximately half in the span of a few weeks. In contrast, other subtypes such as $CD4^+$ TEMRA (min=0.02% to max=0.62%) and neutrophils (min=3.9% to max=31.8%) varied week-to-week by a similar order of magnitude (i.e., 10-fold) as observed between-person in the cohort (see Figure 1e and Supplemental Table 2). Antibody-producing B cells, which had the highest mtDNAcn, varied by up to 1.1-fold (min=0.86% to max=1.8%). Together, these time-course results illustrate the dynamic remodeling of circulating leukocyte populations within a single person. In addition, these data suggest that cell mixtures (e.g. PBMCs) are likely to be confounded by unequal abundance of different cell types on each occasion of sampling.

To ascertain this point, we repeated our analysis above to quantify the influence of circulating abundance on individual mitochondrial metrics in PBMCs within-person. Interestingly, the pattern of associations between mitochondrial features and PBMC mitochondrial function was markedly different between the cohort and repeat participant (Supplemental Figure 7a). Contrary to the cohort, at the within-person level B cell abundance did not correlate with PBMCs mtDNAcn or enzymatic activities, possibly because of the limited range in circulating B cell abundance (only 0.95% week-to-week range in the repeat participant vs 15% range in the cohort). Within-person, the abundance of $CD4^+$ naïve T cells was positively correlated with PBMCs mtDNAcn, CS and CI activity, similar in direction to what we observed at the group level. However, on average, compared to the cohort, the associations between the proportion of cell subtypes and PBMCs mitochondrial features tended to be predominantly inverse correlations, as shown in Supplemental Figure 7b.

In particular, on weeks when the participant had higher circulating levels of EM and TEMRA $CD4^+$ and $CD8^+$ lymphocytes, most mitochondrial features were considerably lower in PBMCs. Interestingly, the associations were in the opposite direction (positive) for CM subtypes, suggesting a potentially meaningful functional distinction between central and effector memory subtypes in relation to PBMCs cell composition and/or mitochondrial function.

Similarly, the associations between CBC-derived cell proportions and PBMCs mitochondrial features tended to be weaker and in opposite direction at the within-person level compared to the cohort (Supplemental Figure 7c-d). Having established that PBMCs are confounded in several ways when examined in a cohort setting, one interpretation of this confounding pattern comparison at the between-person (i.e., cohort) vs within-person levels is that the nature of the confounds (ie., which cell types predominantly influence PBMCs mitochondrial features) may in fact vary from one individual to the next. But regardless of the interpretation, these data reinforce the notion that PBMCs mitochondrial features are heavily skewed by variable cell type distributions.

Mitochondrial content, mtDNAcn and RC activity exhibit natural week-to-week variation

We then analyzed mitochondrial features reflecting content and RC function in each available cell type across the 9 time points. The first observation was that the robust cell type differences reported above in our cohort were conserved in the repeat participant. Monocytes had the highest RC activity, neutrophils the lowest, and $CD4^+$ and $CD8^+$ T lymphocytes showed intermediate activities. Similarly, the available cell subtype with the highest mtDNAcn was $CD8^+$

naïve T cells (average across 9 weeks=400 copies/cell, 427 in the cohort) and neutrophils exhibited the lowest mtDNAcn in both the repeat participant and the cohort (average=123 copies/cell, 128 in the cohort). We note that B cells were of too low abundance to be included in the repeat participant.

We next focused on variation over time. Within specific cell subtypes, we found that all mitochondrial metrics exhibited substantial weekly variation. Within the same person, different cell types showed week-to-week variation ranging from 7.3 to 21.9% for CS activity, 4.1 to 18.3% for mtDNAcn, 8.4 to 37.5% for CI, 4.1 to 15.3% for CII, and 15.2 to 64.4% for CIV (Figure 7b-f). Similarly, MHI in each subtype varied by 8.3 to 20.6%, with the naïve subsets of $CD4^+$ and $CD8^+$ T lymphocytes exhibiting the largest week-to-week changes (rMSSD=0.28 and 0.22, respectively) (Figure 7g). In most cases, the observed variation was significantly greater than the established technical variation in our assays (see Supplemental Table 3), providing confidence that these changes in mitochondrial content and function over time reflect real biological changes rather than technical variability.

To put this natural biological variation in perspective, we directly compared the inter- and intra- individual variation of mitochondrial metrics. Specifically, we asked: relative to differences observed among a heterogeneous cohort of women and men spanning 4 decades of life, how much do the same metrics naturally vary within a single person. Remarkably, for several mitochondrial metrics, the 9-week range of natural variation within the same person was similar to the between-person differences among our 21-participant cohort. Figure 7h provides a side-by-side comparison of the cohort and repeat participant CS activity on the same scale. The C.V. of CS in monocytes was 17.0% for the cohort and 20.2% in the repeat participant. Similarly, in $CD4^+$ naïve T cells, the dynamic range for CS activity among both the cohort and repeat participant was similar. Supplemental Figure 8 shows side-by-side comparisons of between- and within-person variation for other mitochondrial features (mtDNAcn, CI, CII, CIV, and MHI). The similar degree of variation in the repeat participant as in the heterogenous cohort indicates that dynamic variation in mitochondrial function is a generalizable property across all mitochondrial features examined. This also suggests that to ensure the reliability of mitochondrial content and function features, future research may need to incorporate repeated, within-person measures.

When evaluating the stability of PBMCs mitochondrial metrics, we found that PBMCs CS activity, mtDNAcn, and RC activity varied by 9.8-61.9%, similar to the variation observed in isolated subtypes (Figure 7b-g). For mtDNAcn, CI, and CII activities, PBMCs showed either

similar or higher week-to-week variation than neutrophils, the cell subtype with the greatest dynamic variation on these mitochondrial features (despite the absence of neutrophils in PBMCs). Thus, PBMCs exhibit at least an equivalent degree of dynamic variation over time as individual cell subtypes, although again this variation is driven in large part by variation in cell distribution.

Co-regulation of mitochondrial features across cell types

Next, we assessed the co-regulation of mitochondrial content and RC activity across cell subtypes and PBMCs within the same person over time. Despite the small number of timepoints for these comparisons, similar to our cohort findings, CS and mtDNAcn were most highly correlated across cell types (average $r_{z'}$=0.55-0.70) (Figure 7i-j). Again, RC activities were only moderately correlated, indicating partial co-regulation of mitochondrial energetics across some cell subtypes. Of the RC complexes, CI was the most consistent across cell subtypes (average $r_{z'}$=0.39), whereas CIV showed the least co-regulation (average $r_{z'}$=0.06) including several negative correlations (Figure 7j). For example, on weeks when CIV activity for this individual increased in monocytes, CIV activity tended to similarly increase in $CD4^+$ CM-EM T cells (r=0.71, p=0.088), but tended to decrease in $CD8^+$ naïve T cells (r=-0.68, p=0.11). Altogether, these within-person data were consistent with our cohort findings (between individuals), indicating partial co-regulation of mitochondrial features across cell subtypes, including some negative associations that remain unexplained.

Cell type-to-PBMCs associations tended to be stronger in the repeat participant compared to the cohort (Figure 7i, Supplemental Figure 7e-f). In particular, CS activity and mtDNAcn were highly correlated between PBMCs and innate immune cells, even if those cells are only partially contained in PBMCs. In contrast, the associations of mitochondrial features in PBMCs with naïve and memory lymphocytes were more modest, even though lymphocytes are expected to constitute the largest cellular fraction in PBMCs. Thus, PBMCs exhibit substantial dynamic changes among several mitochondrial features that appear relatively independent from those same features in lymphocyte populations, again suggesting a substantial influence of cell distribution and possibly other unknown factors.

Compiling all cell subtype pairs for each mitochondrial feature, we then systematically evaluated the level of agreement between the cohort and the repeat participant. In other words, we asked if two cell subtypes (e.g., $CD4^+$ and $CD8^+$ naïve) are highly correlated for a given mitochondrial feature (e.g., CS) among the cohort, do these cell subtypes also show high correlation within a single person over time? The presence of most datapoints in the upper right

quadrants of Figure 7k supports the general conclusion that mitochondrial features – particularly CS and mtDNAcn – are generally co-regulated across cell types within both the cohort and a single person over time. However, the level of agreement between the cohort and repeat participant was generally weak to medium (r=0.08-0.35, absolute values), possibly pointing to person-level differences in how mitochondrial behavior among different cell types relate to each other.

These and previous results differed by mitochondrial feature, and each feature reflects a slightly different aspect of mitochondrial biology. In previous work[27, 46], combining multiple mitochondrial features into multivariate indices also showed potential to more reliably detect meaningful treatment or group differences. Therefore, in keeping with the concept of mitochondrial functional specialization, we then performed exploratory analyses of cell subtype-specific mitochondrial phenotypes, or *mitotypes*, by mathematically combining multiple mitochondrial features in graphical representation.

Mitotypes differ between immune cell subtypes

As in other complex biological systems, the function and behavior of mitochondria require synergy among multiple features. Therefore, the functional characteristics of mitochondria can be expressed by multivariate indices reflecting the inter-relations of multiple mitochondrial features. This logic is similar to body mass index (BMI), which integrates height and weight into a BMI ratio that is more easily interpretable and meaningful than either height or weight features alone. In relation to mitochondria, in human tissues the ratio of CIV and CII activities (also known as COX/SDH ratio) is used in diagnoses of mitochondrial dysfunction, whereas alone either CIV or CII activities are less easily interpretable[47]. Thus, integrating primary features of mitochondrial content, genome abundance, and RC function could produce integrated *mitotypes*, which reflect the functional specialization of mitochondria among different cell subtypes, or among dynamic cellular states.

Similar to BMI, the mitotypes analyzed (listed and defined in Supplemental Figure 9) are computed from the ratio of two or more mitochondrial features. Each mitotype can be visualized as a scatterplot with two variables of interest as the x and y axes (Figure 8a). In the example in Figure 8a, the hypothetical cell type A has a higher value for feature 2 relative to feature 1 (Mitotype A), while cell type B has a higher value for feature 1 relative to feature 2 (Mitotype B). Note that if both features increase or decrease following the same proportions, the ratio is the same and follows a diagonal line on the mitotype graph, reflecting an invariant mitotype. Thus,

similar to BMI, changes in mitotypes are reflected by perpendicular movement relative to the diagonal in the mitotype space.

Given that leukocyte subtypes differ widely in their bioenergetic properties, we asked in our cohort (n=21 individuals) if different cell subtypes have different mitotypes. The first mitotype examined puts in relation mtDNA copies per cell (mtDNAcn) relative to mitochondrial content per cell (CS activity), creating a mitotype (mtDNAcn/CS) reflecting *mtDNA density per mitochondrion* (Figure 8b). Alone, this mtDNA density per mitochondrion mitotype provided remarkable separation of cell subtypes. Neutrophils and NK cells were low on both metrics, B cells were high on both metrics, monocytes had the lowest mtDNA density, whereas $CD8^+$ naïve T cells exhibited the highest mtDNA density of all cell subtypes tested. Figures 8c-e illustrate other mitotypes including i) CII activity per unit of mitochondrial genome (CII/mtDNAcn), as well as more complex combinations of variables such as ii) CI activity per mtDNA (CI/mtDNAcn ratio on y axis) in relation to mtDNA density (mtDNAcn/CS activity on x axis), and iii) CI activity per mitochondrial content (CI/CS, y axis) in relation to mtDNA density (mtDNAcn/CS, x axis). As Figure 8b-e shows, PBMCs generally exhibit a similar mitotype (diagonal line from the origin of the plot) as innate immune cell subtypes (monocytes, NK cells, and neutrophils), and are relatively distinct from lymphocyte subpopulations. We understand these mitotype combinations to reflect the well-known principles of mitochondrial functional specialization[17, 48] and to represent individual mitochondrial “personality types" tailored to subserve specific bioenergetic and biosynthetic requirements within immune cell subtypes.

This mitotype-based analysis of mitochondrial characteristics revealed two main points. First, cells of the innate and adaptive immune subdivisions contain mitochondria that differ not only quantitatively in their individual metrics of mitochondrial content and RC activity, but that exhibit marked qualitative differences. This is illustrated by the distinct clustering of neutrophils, monocytes and NK cells (innate) within similar mitotype spaces, and the clustering of all lymphocyte subtypes together in a different space. Compared to cells of the innate immune compartment, lymphocytes (adaptive) had higher mtDNAcn and lower respiratory chain activity. A second insight from this analysis is that compared to naïve subsets of $CD4^+$ and $CD8^+$ T cells, which themselves have relatively distinct mitotypes (e.g., CII/mtDNAcn, Figure 8c), both memory $CD4^+$ and $CD8^+$ subtypes converged to similar mitotype spaces. Functionally, this naïve-to-memory transition is well known to involve a metabolic shift including changes in spare respiratory capacity, mitochondrial content, glucose and fatty acid uptake[41, 49]. The mitotype analysis showed that compared to naïve cell subtypes, memory subtypes exhibit 26-29% lower mtDNA density per

mitochondrion, but an 8-23% increase in RC activity per mitochondrion in $CD4^+$ T cells, although not in $CD8^+$ T cells (Figure 8f).

Stability of mitotypes

Next, we examined how stable these cell-type specific mitotypes were in the independent repeat participant dataset. We plotted matching cell types for the cohort and for the repeat participant on the same mitotype plots. As evidenced in the cohort, cell types belonging to the innate and adaptive immune subdivisions similarly clustered together, and naïve and memory subtype differences were similarly validated at the within-person level (Figure 8g-i), demonstrating the conserved nature of immune cell mitotypes.

To examine the biological stability of mitotypes across individuals, we determined the effect sizes between cell subtypes for selected mitotypes in our cohort, and then compared these to the magnitude of the differences between the cohort and the repeat participant for specific cell subtypes (Figure 8j). First, consistent with the results for individual mitochondrial features (see Figure 4), the effect sizes comparing mitotypes between cell subtypes ranged from moderate to very large. For example, mitotype differences between monocytes and $CD8^+$ naïve T lymphocytes had effect sizes ranging from g=2.5 to 3.5. Neutrophils and NK cells, which were among the most similar cell types on most mitotype plots, had Hedges' g values ranging from 0.2 (small) to 1.2 (very large), reflecting considerable mitotype differences even among these cell types. In comparison, inter-individual variation (cohort n=21 vs repeat n=9) across different mitotypes was over an order of magnitude smaller, with pooled effects sizes being on average 12.5-fold smaller than were cell type differences. Overall, these data across both the mixed cohort of women and men, and the within-person repeated-measures, reveal that immune cell subtypes have distinct and robust mitotypes consistent with their divergent bioenergetic requirements.

Evidence for a sex and age bias in mitotypes

We next sought to systematically examine if mitotypes differ between women and men. Mitotypes were organized into five categories of indices based upon their features, yielding a total of 16 mathematically-distinct mitotypes (see Supplemental Figure 9). For each mitotype, we quantified the magnitude of the difference between women and men by the effect size (g), ranked all mitotype x cell subtype combinations (16 mitotypes x 9 cell subtypes), and analyzed the distribution of these indices by sex. The majority of mitotypes reflecting mitochondrial RC activities per CS activity were higher in men ($p<0.0001$, Chi-square), while RC activity per mtDNA density ($p<0.001$) and RC activity per genome in relation to mtDNA density mitotypes ($p<0.01$) were

predominantly higher in women (Figure 9a). The magnitude of sex differences ranged from 17% higher in men (CI/CS in $CD4^+$ CM-EM T cells, g=1.14) to 38% higher in women (CII/mtDNA density in neutrophils, g=1.37) (Figure 9b). The direction of sex differences for all mitotypes (e.g. higher in women or in men) with effect sizes is illustrated in Figure 9c**.** The average effect size across all mitotypes was 0.31 (small) in $CD4^+$ naïve T cells, compared to monocytes where the average effect size was 0.71 (medium). Compared to purified cell subtypes, the magnitude of sex differences in the PBMCs cell mixture appeared blunted.

Using the same approach, we then systematically quantified the relationship between mitotypes and age. Mitotypes reflecting RC activity per CS activity were predominantly positively correlated with age (p=0.046), while RC activities per genome in relation to mtDNA density were generally negatively correlated with age (p=0.012) (Figure 9d). This finding is consistent with the overall age-related increase in mtDNAcn across cell subtypes, and could indicate a general decrease in the RC output per unit of mitochondrial genome with aging in immune cells. The strength of these correlations ranged from r=-0.67 to 0.75 (Figure 9e). The correlations of individual mitotypes with age for each cell subtype are shown in Figure 9f. Again, PBMCs showed among the weakest associations with either sex or age (Figure 9c and f). Thus, even if specific cell subtypes reveal consistent sex- and age-related differences, PBMCs offer modest to no sensitivity to detect these associations.

Overall, these findings reveal consistent patterns of differences in immune cell mitotypes between women and men, and to a lesser extent with aging. Importantly, these data also indicate that the observed differences vary considerably by cell subtype. Whereas innate immune cells exhibited the strongest sex differences, B cells exhibited the largest age-related mitotype changes.

Associations of blood biomarkers with subtype-specific mitochondrial features

To explore the source of inter-individual differences and within-person dynamics over time described above, we asked to what extent subtype-specific mitochondrial features were correlated with blood biomarkers. We examined a panel of sex hormones, inflammatory markers, metabolic markers, and standard clinical blood biochemistry in relation to subtype-specific mitochondrial features (Figure 10a). Because mitochondrial features in specific cell types, as well as blood biomarkers, were both associated with sex and age, we examined sex- and age-adjusted partial correlations. At the cohort level, associations between blood biomarkers and cell subtype mitochondrial phenotypes were relatively weak (Figure 10b), indicating that circulating neuroendocrine, metabolic and inflammatory factors are unlikely to explain a large fraction of the

variance in inter-individual differences in mitochondrial biology, pointing instead to behavioral, genetic and other influences as the source of inter-individual variation.

We then examined this question at the within-person level where week-to-week variation is independent of constitutional and genetic influences, and where behavior (e.g., levels of physical activity, sleep patterns, etc.) is more stable relative to the behavioral differences between women and men of different ages. Compared to the cohort, the strength of associations between biomarkers and mitochondrial metrics across cell types was on average 0.7-fold larger in the repeat participant (average absolute values, $r_{z'}$=0.39 for the repeat participant vs 0.23 for the cohort) (Figure 10c). Another notable finding was the difference in the correlation patterns between biomarkers and different cell subtypes. These cell-type specific correlation patterns are consistent with differences either in mitochondria themselves, or in other properties of the cells that host them, which may exhibit different sensitivities to circulating neuroendocrine, metabolic, or biochemical factors.

Notable patterns of associations between circulating biomarkers and mitochondrial features emerged at the within-person level. For instance, lipid levels including triglycerides, total cholesterol, and low- and high-density lipoproteins (LDL, HDL) were positively correlated with markers of mitochondrial content (CS activity and mtDNAcn), with the largest effect sizes observed among innate immune cells: neutrophils, NK cells, and monocytes (Figure 10c, red area on the heatmap). In these cells, lipid levels accounted on average for 53% of the variance (r^2) in CS activity and 47% in mtDNAcn. We note that some of these estimates are likely overestimated due to the small number of repeated measures. Compared to CS and mtDNAcn, these associations were less consistent for RC enzyme activities and MHI. We speculate that the positive association of lipid levels and mitochondrial content features in innate immune cells could reflect the action of lipid signaling pathways well known to stimulate mitochondrial biogenesis in various tissue types[47, 50, 51, 52].

We finally examined potential divergences in the associations among the cohort compared to the repeat participant. It is established that different individuals show remarkably different baseline levels of both mitochondrial features and blood biochemistry measures (e.g., some people have higher blood cholesterol than others). Moreover, our data shows that within a person, there is also extensive physiological variation in mitochondrial features and in blood biochemistry over time. Therefore, we reasoned that *even* if each participant in our cohort was to exhibit a strong positive correlation between LDL and CS activity over time, sampling each person on a

single randomly selected occasion (where LDL could substantially differ) would not reveal this positive correlation at the cohort or group level. As an illustration of this point, in the repeat participant we found a strong association between lipids and mitochondrial content (LDL and neutrophil CS activity, $r=0.90$, $p<0.01$) that was not observed in the cohort, where each datapoint represents a single time point for a given person (panel 1 of Figure 10d). The lack of association in the cohort was apparent despite a substantially larger dynamic range in LDL in the cohort relative to the repeat participant (43-180 vs 105-134 mg/dL, respectively). On the other hand, between-person comparisons in the cohort also revealed apparent associations that were not observed in the repeat participant (Figure 10d, panels 3 and 4).

Altogether, although suggestive and not definitive, the divergence in the correlation strengths and patterns between the cohort and repeat participant (Figure 10e) again highlight the potential value of repeated-measures designs to examine the influence of humoral factors on immune mitochondrial biology.

Discussion

Mapping the naturally occurring bioenergetic differences among various tissues and cell types is critical to further our understanding of the role of mitochondria in human health and disease. Here we have used the immune system as a model to examine this question, isolating and phenotyping multiple immune cell subtypes and mixed PBMCs among a diverse cohort of women and men, and in repeated weekly measures in the same participant. Our study first described wide variation in the proportions of circulating innate and adaptive cell subtypes, both between and within-person. Using a high-throughput mitochondrial phenotyping platform, we define large functional differences between immune cell subtypes in mitochondrial features reflecting both mitochondrial content and respiratory chain function. These mitochondrial features also vary moderately by age and sex, but only when examined in purified cell populations. Importantly, our results show that PBMCs mitochondrial measurements are confounded in multiple ways including i) cell type composition, ii) platelet contamination, iii) mitochondrial properties across different cell subtypes, and iv) the dynamic remodeling of cell type composition and bioenergetics over time. As a result, PBMCs largely mask age- and sex-related changes in immune mitochondrial biology. In addition, we uncover large week-to-week within-person variation in both cell subtype proportions and mitochondrial behavior, pointing to heretofore underappreciated dynamic regulation of mitochondrial content and function over time. Finally, as

a first step towards identifying stable cell-type specific bioenergetic profiles for future research, we also introduce multivariate mitotypes. These data in specific leukocyte populations provide foundational knowledge of mitochondrial phenotypes in human immune cells, their sensitivity to inter-individual variables such as age and sex, and highlight the value of repeated-measures designs to examine the mechanisms of dynamic mitochondrial variation in humans.

Because PBMCs are widely used across fields, mostly due to their ease of collection, we wanted to examine whether they would reflect or mask observations in specific cell subtypes. In many cases, associations with moderate to large effect sizes in specific cell subtypes were either not observed or blunted in PBMCs. For example, there was no correlation between age and PBMCs MHI either in this study or previously[53], but correlations were present in purified cell subtypes. Interestingly, the mitotype analysis revealed similar mitotypes between total PBMCs and cells of the innate subdivision, namely neutrophils, NK cells, and monocytes (often aligned along the same mitotype diagonal space on mitotype plots). In the mitotype plots, if PBMCs were composed uniquely of a mixture of lymphocytes and monocytes, the natural expectation is that PBMCs would lie somewhere between the specific subsets that compose it. Instead, PBMCs occupy an entirely different and unexpected mitotype space, indicating the presence of one or more contaminating factors. Our platelet depletion experiment, even if we started with platelet-depleted PBMCs (Ficoll plus two low spin centrifugation steps) leaves little doubt that platelet contamination skews the measurements of several mitochondrial features in PBMCs, with some features being apparently more affected than others. This could explain the discrepancies between PBMCs and purified cell types, including why PBMCs have higher CS activity values than any of its constituent cells. Although we cannot entirely rule out potential contamination of individual cell types with residual platelets, the FACS labeling, washing, and sorting procedures produce the purest sample with the highest degree of biological specificity.

However, a major frontier for the human immunometabolism field consists in defining temporal trajectories of change over time in specific cell types[54]. Achieving this goal promises to transform our knowledge of immune and mitochondrial biology, and allow for the rational design of therapeutic approaches[54]. A primary finding of our work is a natural within-person variation of mitochondrial features, providing initial insight into the temporal dynamics of immunometabolism in specific human cell subtype populations. Sorting of immunologically-defined cell subtypes removes the potential confound of week-to-week changes in cell type distributions, an inherent confounding variable in PBMCs, and therefore adds confidence in the robustness of the reported temporal mitochondrial variation. This within-person analysis revealed that mitochondrial features

within immune cells exhibit state-like properties that vary by >20-30% week-to-week. These findings warrant future studies investigating the factors that drive these changes. We had previously observed in PBMCs that up to 12% of the inter-individual variation in MHI was attributable to positive mood (ratings of positive experiences such as excited, hopeful, inspired, love) the night prior blood draw[27], implying that psychosocial factors could in part contribute to a substantial portion of the dynamic variation in leukocyte mitochondrial function over 24 hours. However, limitations in this prior study – including the use of PBMCs and a single measurement time point for MHI – call for additional work to disentangle the independent contributions of behavioral, psychosocial, nutritional, and other factors on mitochondrial features in humans. Importantly, our results demonstrate that mitochondrial changes are taking place within less than one week. Therefore, we posit that establishing the exact temporal dynamics of leukocyte mitochondrial variations and immunometabolism in general will require repeated assessments with even higher temporal resolution.

A particularly striking observation is that, in some cell types, the dynamic changes in cell subtype-specific mitochondrial features within a person can, in some cell types, be of similar magnitude to the biological variation observed between people (i.e., among a heterogenous reference cohort of 21 individuals composed of women and men spanning four decades of life). Thus, a single measure of mitochondrial function may not accurately reflect a given person's average mitochondrial functional capacity. Therefore, as for other biological markers with high intra-individual variability (e.g., cortisol[55]), our results highlight the importance of repeated-measures designs to reliably capture stable inter-individual differences in future research.

Our exploratory mitotype approach provided further insight on the mitochondrial functional specialization among circulating human immune cell subtypes. Most notably, the innate and adaptive subdivisions, as well as the metabolic transition from naïve T lymphocytes to memory states, harbored distinct mitotypes. Mitotypes of specific cell subtypes were also relatively conserved between our heterogenous cohort and repeat participant. Moreover, the mitotype analysis revealed potentially generalizable sex- and age-related differences in mitochondrial features. Thus, the mitotype approach may help to achieve an understanding of both quantitative and qualitative differences in mitochondrial phenotypes.

In relation to sex differences, animal studies have consistently identified sexually dimorphic mitochondrial features, including greater mitochondrial content in females (reviewed in [56]). Likewise, a study in humans showed that PBMCs from women have greater CS activity, and

greater CI and CII-mediated respiration[57]. Consistent with previous findings, our data show similar changes in enzymatic activities for most, but not all cell types, suggesting that the magnitude of sex differences is likely cell-type specific. Therefore, the use of methods offering a sufficient level of biological specificity appear warranted to reproducibly and accurately quantify these sex differences in different contexts.

In relation to age, previous studies in whole blood[38, 39], PBMCs[40], and skeletal muscle tissue[58, 59], but not liver[60], have consistently reported an age-related decline in mtDNAcn. However, these studies, particularly those in blood, are confounded by the existence of cell mixtures and platelet contamination[12, 13]. For example, in a study of 672 adults, accounting for cell type distribution and platelet count through measurement and statistical adjustments eliminated initial associations between mtDNAcn and age[61]. Our data, like previous studies[11, 12, 13, 14], demonstrate how platelets inflate mtDNAcn, as well as other mitochondrial features. Integration of data across two population-based studies and our cohort show that platelet number consistently decreases with age, which could account for the apparent decline in blood or PBMCs mtDNAcn when sampling individuals across the lifespan – older individuals have fewer platelets, and therefore appear to have less mtDNA copies per cell, even if cellular mtDNAcn is actually unchanged. In fact, our cell-specific data shows that cellular mtDNAcn is positively correlated with age – increasing by as much as 10% per decade between ages 20 to 60. Given the accumulation of mtDNA mutations and deletions with age (e.g.,[40, 62]), and that mtDNA defects can trigger the compensatory upregulation of mtDNAcn to counteract the loss of intact mitochondria associated with age[63, 64], the observed positive correlation of mtDNAcn with age could reflect compensatory upregulation of mtDNA replication. Alternatively, this could reflect impaired autophagic removal in aging cells, an interpretation consistent with recent results in CD4+ T cells[24]. The only cell type examined that did not exhibit an age-related positive association with mtDNAcn are $CD8^+$ naïve T cells, which, interestingly, is the only cell type whose abundance in circulation significantly declines with advancing age. The basis for the direction of this association requires further investigation.

This study presents limitations that should be noted. First, although this represents, to our knowledge, the largest available study of mitochondrial biochemistry and qPCR in hundreds of samples, the cohort is of relatively small size and the exhaustive repeated-measures was carried out in only one participant. We included an equal representation of women and men in the cohort, but the sample size precluded stratification of all analyses by sex. Additionally, because our mitochondrial phenotyping platform currently requires ~5 million cells per sample, we only

collected the six most abundant cell subtypes from each participant, which in some instances reduced the final sample size for different cell subtypes. The variable proportions of cell subtypes from person-to-person are provided in Supplemental Table 2, which determined which cell subtypes were collected from each participant. In order to accommodate the minimum cell number per sample, CM and EM subtypes were grouped, although they may exhibit differences not examined here. Furthermore, we recognize that additional cell surface markers may be useful to identify cell populations not included here (e.g., activated or adaptive lymphocyte subtypes). Finally, we did not test participants for CMV status, which could contribute to the age-related effects on immune cell subtypes.

Altogether, these mitochondrial profiling results in circulating human immune cells fill three main knowledge gaps. (1) They define confounds for PBMCs and show how PBMCs fail to capture age- and sex-related mitochondrial recalibrations that exist in specific immune cell populations, an important finding for the design of future studies. (2) They precisely document large-scale, quantitative differences in CS activity, mtDNAcn, and RC function between immune cell subtypes, which represent foundational knowledge of the metabolic characteristics in key cell types in the human immune system. Additionally, our mitotype approach identifies conserved multivariate phenotypic distinctions between lymphoid and myeloid cells, and naïve-to-memory lymphocyte states. Finally, (3) this work reveals dynamic variation in mitochondrial function, providing initial evidence of the natural within-person variation of cell subtypes and dynamic mitochondrial profiles over days to weeks. These results provide the required foundational knowledge to develop interpretable blood-based assays of mitochondrial health.

Methods

Participants

The study was approved by New York State Psychiatric Institute (Protocol #7618). All participants provided written informed consent. Healthy adults between 20 and 60 years willing to donate blood were eligible for inclusion. Exclusion criteria included severe cognitive deficit, symptoms of flu or other seasonal infection four weeks preceding the visit, involvement in other clinical trials, malignancy or other clinical condition, and diagnosis of mitochondrial disease. Participants were recruited via flyers posted in the Columbia University Irving Medical Center (CUIMC) community. Participants completed a short demographic questionnaire, anthropometric measurements (weight, height, heart rate, and blood pressure), and a blood draw. The main study cohort included twenty-one individuals (11 women, 10 men), mean age 36 ±11 (SD, range: 23-57), were recruited. The ethnic breakdown of our sample was: 2 African Americans, 7 Asians, and 12 Caucasians. All blood draws took place in the morning between 9-10am. Additionally, repeated weekly measures were collected across 9 weeks from one healthy Caucasian man (author M.P., 34 years old) to assess within-person variability in mitochondrial measures and immune cell type distribution. To standardize and minimize the influence of nutritional and behavioral factors in the repeat participant, repeated measures were collected at the same time (9:00am), on the same day of the week (Fridays), after a standardized breakfast (chocolate crepe), ~30-60 minutes after a regular bicycle commute to study site.

Blood Collection

*A total o*f 100 ml of blood was drawn from the antecubital vein for each participant and included one EDTA tube (Cat# BD367841, 2 ml) for complete blood count (CBC), two SST coated tubes (Cat#BD367986, 5 ml) for hormonal measures and blood biochemistry in serum, and 11 Acid Dextrose A (ACD-A) tubes (Cat# BD364606, 8.5 ml) for leukocyte isolation and mitochondrial analyses, in order of collection. All tubes were gently inverted 10-12 times immediately after draw to ensure proper mixing. The EDTA and SST tubes for hematological and blood biochemistry were processed by the Center for Advanced Laboratory Medicine (CALM) Lab, and the ACD-A tubes were further processed for cell isolation.

PBMCs and leukocyte isolation

Ficoll 1077 and 1119 (Sigma), Hanks Balanced Salt Sodium (HBSS) without phenol red, calcium and magnesium (Life Technologies, Cat# 14175103) supplemented with 2% BSA (Sigma, Cat# A9576) (HBSS/BSA), HBSS/BSA supplemented with 1 mM of EDTA (Sigma, Cat# E9884)

(HBSS/BSA/EDTA), and FBS (Thermofisher, cat# 10437036) were brought to room temperature overnight. PBMCs were isolated on 15 ml of low density Ficoll 1077 in a 50 ml conical tube, and total leukocytes were separated on 15ml of higher density Ficoll 1119 distributed across 7 conical tubes. Blood was first pooled and diluted with HBSS/BSA in a 1:1 ratio, and 25 ml of diluted blood was carefully layered on Ficoll and then centrifuged immediately at 700 x g for 30 minutes (no brake) in a horizontal rotor (swing-out head) tabletop centrifuge, at room temperature. Immediately after centrifugation, cells at the interface were collected and washed in 50 ml HBSS/BSA and centrifuged at 700 x g for 10 minutes. Supernatants were discarded and leukocyte pellets washed again in HBSS/BSA/EDTA and centrifuged at 700 x g for 10 minutes to limit platelet contamination. Low concentration EDTA (1mM) was used to prevent cell-cell adhesion or platelet activation, but a higher concentration was not used to avoid perturbing downstream mitochondrial assays.

To perform cell count, both i) PBMCs (1:10 dilution) and ii) total leukocytes (1:100 dilution) were resuspended in 1 ml of HBSS/BSA/EDTA and counted on the Countess II FL Automated Cell Counter (Thermo Fisher Scientific, Cat# AMQAF1000) in a 1:1 dilution with trypan blue. Counts were performed in duplicates. If the difference between duplicates >10%, the count was repeated and the grand mean of the cell counts taken. Pellets of 5 million PBMCs were aliquoted and frozen at -80°C for mitochondrial assays.

Immunolabeling of cell surface markers

Two antibody cocktails meant for i) cell counting (Cocktail 1) and ii) cell sorting (Cocktail 2), were prepared for fluorescence-activated cell sorting (FACS) (see Supplemental Table 4 for details). Antibodies were gently mixed, kept at 4°C, and shielded from light to avoid bleaching. Cocktail 1 (containing cell surface markers for activated T lymphocytes) was prepared with 17.5 ul HBSS/BSA/EDTA and 2.5 ul per antibody (13 markers, 32.5 ul total antibody mix), for a total of 50 ul. Cocktail 2 was prepared with 200 ul HBSS/BSA/EDTA and 25 ul per antibody (12 markers, 300 ul total sorting antibody mix), for a total of 500 ul.

Prior to each study visit, cell collection tubes (Cat#: 352063, polypropylene, 5 ml) were coated with 4.5ml of DMEM/10% FBS media to minimize cell-tube adhesion and maximize the recovery of sorted cells. Tubes were incubated for 24 hours at room temperature and stored at 4°C until use, and decanted prior to use. Two coated polypropylene tubes were used for the FACS-ready antibody-labeled leukocytes, and an additional 60 coated polypropylene falcon tubes were decanted and 500 ul of media (DMEM/10% FBS) was added to receive sorted cells.

Prior to immunolabeling, total leukocytes were incubated with blocking buffer (to block non-specific binding to FC receptors) at a 1:10 dilution and incubated at room temperature for 10 minutes. A 2 million cell aliquot was diluted to a final volume of 100 ul with HBSS/BSA/EDTA and combined with 50 ul of Cocktail 1. The remainder of total leukocytes (~100M cells) were incubated with 500 ul of Cocktail 2 for 20 minutes in the dark, at room temperature. Both cell preparations were then washed with 5 ml of HBSS/BSA/EDTA and centrifuged at 700 x g for 5 minutes. Using the propylene tubes, Cocktail 1 cells were resuspended in 200 ul of HBSS/BSA/EDTA, and total leukocytes for FACS were resuspended to final concentration of 20 million cells/ml with HBSS/BSA/EDTA.

Fluorescence-activated cell sorting (FACS)

Cells labeled with the Cocktail 1 (counting) panel was only used for data acquisition and phenotype analysis. Cells labeled with the Cocktail 2 (sorting) panel was FACS sorted using a BD™ Influx cell sorter to isolate the subpopulations from peripheral blood. The sorter was controlled using BD FACS Sortware. Cells were sorted using 100 um size nozzle and under the sheath pressure of 20 psi. Sorting speed was kept around 11,000-12,000 events/second. Cell concentration for sorting was measured at about $15x10^6$ cells per ml. Cell sorter drop frequency was 37 KHz, stream focus was 10%, maximum drop charge was 110 Volts. A six-way sorting, 1.0 drop pure sort mode was used to sort the cell subpopulations. Stream deflections were -84, -65, -32, 32, 65, and 84 for six-way sort from left to right. For each participant, 1 million cells (Cocktail 1 panel) were run first to calculate the potential yield of each subpopulation, including neutrophils, B cells monocytes, NK cells, naïve $CD4^+$ and $CD8^+$, CM $CD4^+$ and $CD8^+$, EM $CD4^+$ and $CD8^+$, and TEMRA $CD4^+$ and $CD8^+$ (total cell number x percentage of each subpopulation). The six most abundant subpopulations were sorted. Purity checks were performed on all sorted subpopulations to ensure the instrument performance was good enough to reach the sorted population purity >95%. Raw data (.fcs file) was exported for further analysis on FCS Express 7 research version.

Processing and storage of sorted cells

Following flow cytometry, sorted cell subtypes were transferred and pooled by pipetting about half of each collection tube (2.5 ml) into larger falcon tubes, gently vortexing to liberate cells that may have adhered to the tube wall, and the remaining volume pipetted into the transfer tube. HBSS/2% BSA was used as necessary to equilibrate and cells were centrifuged at 1,000 x g for 5 minutes. Following centrifugation, each cell pellet was isolated by gently decanting the supernatant and re-suspended into 1ml of HBSS/2% BSA. The resulting purified cell suspensions were transferred to a 1.5 ml Eppendorf tube for each cell type, centrifuged at 2,000 x g for 2

minutes at 4°C, and the supernatant carefully removed to leave a dry cell pellet. Samples were stored in liquid nitrogen for 4-12 months (-170°C) until mitochondrial biochemistry and mtDNAcn analyses were performed as a single batch.

Mitochondrial enzymatic activities

Samples were thawed and homogenized in preparation for enzymatic activity measurements with one tungsten bead and 500 ul of homogenization buffer (1 mM EDTA, 50 mM Triethanolamine). Tubes were transferred to a pre-chilled rack and homogenized using a Tissue Lyser (Qiagen cat# 85300) at 30 cycles/second for 1 minute. Samples were then incubated for 5 minutes at 4°C, and homogenization was repeated for 1 minute and the samples were returned to ice ready for enzymatic assays.

Mitochondrial enzyme activities were quantified spectrophotometrically for citrate synthase (CS), cytochrome c oxidase (COX, Complex IV), succinate dehydrogenase (SDH, Complex II), and NADH dehydrogenase (Complex I) as described previously[27] with minor modifications. Each sample was measured in triplicates for each enzymatic assay (3 wells for total activity and 3 wells for non-specific activity, except for the COX assay where a single non-specific activity value is determined across 30 wells). Homogenate volumes used for each reaction were: CS: 10 ul, COX and SDH: 20 ul, Complex I: 15 ul.

CS activity was measured by detecting the increase in absorbance at 412 nm, in a reaction buffer (200 mM Tris, pH 7.4) containing acetyl-CoA 0.2 mM, 0.2 mM 5,5'- dithiobis-(2-nitrobenzoic acid) (DTNB), 0.55 mM oxaloacetic acid, and 0.1% Triton X-100. Final CS activity was obtained by integrating OD^{412} change from 150-480 sec, and by subtracting the non-specific activity measured in the absence of oxaloacetate. COX activity was measured by detecting the decrease in absorbance at 550 nm, in a 100 mM potassium phosphate reaction buffer (pH 7.5) containing 0.1% n-dodecylmaltoside and 100 μM of purified reduced cytochrome c. Final COX activity was obtained by integrating OD^{550} change over 200-600 sec and by subtracting spontaneous cyt c oxidation without cell lysate. SDH activity was measured by detecting the decrease in absorbance at 600 nm, in potassium phosphate 100 mM reaction buffer (pH 7.5) containing 2 mM EDTA, 1 mg/ml bovine serum albumin (BSA), 4 μM rotenone, 10 mM succinate, 0.25 mM potassium cyanide, 100 μM decylubuquinone, 100 μM DCIP, 200 μM ATP, 0.4 μM antimycin A. Final SDH activity was obtained by integrating OD^{600} change over 200-900 sec and by subtracting activity detected in the presence of malonate (5 mM), a specific inhibitor of SDH. Complex I activity was measured by detecting the decrease in absorbance at 600 nm, in potassium phosphate 100 mM

reaction buffer (pH 7.5) containing 2 mM EDTA, 3.5 mg/ml bovine serum albumin (BSA), 0.25 mM potassium cyanide, 100 μM decylubuquinone, 100 μM DCIP, 200 μM NADH, 0.4 μM antimycin A. Final Complex I activity was obtained by integrating OD^{600} change over 120-600 sec and by subtracting activity detected in the presence of rotenone (500 μM) and piericidin A (200 μM), specific inhibitors of Complex I. All assays were performed at 30°C. The molar extinction coefficients used were 13.6 L $mol^{-1}cm^{-1}$ for DTNB, 29.5 L $mol^{-1}cm^{-1}$ for reduced cytochrome c, and 16.3 L $mol^{-1}cm^{-1}$ for DCIP to transform change in OD into enzyme activity.

Mitochondrial enzymatic activities were measured on a total of 340 samples, including 136 replicates of the same cell type for the same person. This provided more stable estimates of enzymatic activities than single measures would for a total of 204 individual person-cell combinations. The technical variation for each enzyme varied according to cell type, with cell types with lower enzymatic activities generally showing the highest coefficient of variation (C.V.). C.V. averaged across all cell types were: CS = 6.3%, Complex I = 16.6%, SDH = 9.3%, COX = 23.4% (Supplemental Table 3).

Mitochondrial DNA copy number

mtDNAcn was determined as described previously[27] with minor modifications. The same homogenate used for enzymatic measurements (20 ul) was lysed in lysis buffer (100 mM Tris HCl pH 8.5, 0.5% Tween 20, and 200 ug/ml proteinase K) for 10 hours at 55°C followed by inactivation at 95°C for 10 minutes. Five ul of the lysate was directly used as template DNA for measurements of mtDNA copy number. qPCR reactions were set up in triplicates using a liquid handling station (ep-Motion5073, Eppendorf) in 384 well qPCR plates. Duplex qPCR reactions with Taqman chemistry were used to simultaneously quantify mitochondrial and nuclear amplicons in the same reactions. *Master Mix$_1$* for ND1 (mtDNA) and B2M (nDNA) included: TaqMan Universal Master mix fast (life technologies #4444964), 300 nM of primers and 100 nM probe (ND1-Fwd: GAGCGATGGTGAGAGCTAAGGT, ND1-Rev: CCCTAAAACCCGCCACATCT, Probe:HEX-CCATCACCCTCTACATCACCGCCC-3IABkFQ.B2M-Fwd:CCAGCAGAGAATGGAAAGTCAA,B2M-Rev: TCTCTCTCCATTCTTCAGTAAGTCAACT, Probe:FAM-ATGTGTCTGGGTTTCATCCATCCGACA-3IABkFQ). *Master Mix$_2$* for COX1 (mtDNA) and RnaseP (nDNA) included: TaqMan Universal Master Mix fast, 300 nM of primers and 100 nM probe (COX1-Fwd: CTAGCAGGTGTCTCCTCTATCT, COX1-Rev: GAGAAGTAGGACTGCTGTGATTAG, Probe: FAM-TGCCATAACCCAATACCAAACGCC-3IABkFQ. RnaseP-Fwd: AGATTTGGACCTGCGAGCG, RnaseP-Rev: GAGCGGCTGTCTCCACAAGT, Probe: FAM-TTCTGACCTGAAGGCTCTGCGCG-3IABkFQ.

The samples were then cycled in a QuantStudio 7 flex qPCR instrument (Applied Biosystems Cat# 4485701) at 50°C for 2 min, 95°C for 20 sec, 95°C for 1 min, 60°C for 20 sec for 40x cycles. Reaction volumes were 20 ul. To ensure comparable Ct values across plates and assays, thresholds for fluorescence detection for both mitochondrial and nuclear amplicons were set to 0.08.

mtDNAcn was calculated using the ΔCt method. The ΔCt was obtained by subtracting the average mtDNA Ct values from the average nDNA Ct values for each pair ND1/B2M and COX1/RNaseP. Relative mitochondrial DNA copies are calculated by raising 2 to the power of the ΔCt and then multiplying by 2 to account for the diploid nature of the nuclear genome (mtDNAcn = 2ΔCt x 2). Both ND1 and COX1 yielded highly correlated mtDNAcn and the average of both amplicon pairs was used as mtDNAcn value for each sample. The overall CV across all cell subtypes was 5.1% for mtDNAcn.

Platelet depletion in PBMCs

For this experiment, participants were 9 community-dwelling older adults (mean age = 79, range: 64-89, 4 women and 5 men). The sample included 7 White and 2 African American participants. Exclusion criteria included diseases or disorders affecting the immune system including autoimmune diseases, cancers, immunosuppressive disorders, or chronic, severe infections; chemotherapy or radiation treatment in the 5 years prior to enrollment; unwillingness to undergo venipuncture; immunomodulatory medications including opioids and steroids; or more than two of the following classes of medications: psychotropics, anti-hypertensives, hormones replacement, or thyroid supplements. Participants were recruited from a volunteer subject pool maintained by the University of Kentucky Sanders-Brown Center on Aging. The study was conducted with the approval of the University of Kentucky Institutional Review Board. Blood (20 mL) was collected by venipuncture into heparinized tubes in the morning hours to control for potential circadian variation. PBMCs were isolated from diluted blood by density gradient centrifugation (20 min at 800 x g, brake off) using Histopaque (Sigma, St. Louis, MO). Buffy coats were washed once, and cells were counted using a hemocytometer. PBMCs (20-30M) were cryopreserved in liquid nitrogen in RPMI-1640 (Lonza) + 10% fetal bovine serum (Hyclone) + 10% DMSO (Fisher), until further processing.

For platelet depletion, PBMCs were first thawed at room temperature and centrifuged at 500 x g for 10 minutes. The supernatant was discarded, and the cells were resuspended in 2 ml of Hank's Balanced Salt Sodium (HBSS) without phenol red, calcium and magnesium (Life

Technologies, Cat#14175103). Cells were then counted on the Countess II FL Automated Cell Counter (Thermo Fisher Scientific, Cat# AMQAF1000) in a 1:1 dilution with trypan blue. Cells were then divided into 2 aliquots: 1) 10 million cells for total PBMCs; 2) 11 million cells for platelet depletion. The total PBMCs were centrifuged at 2,000 x g for 2 min at 4°C and subsequently frozen as a dry pellet at -80°C until processing for enzymatic assays and qPCR. The PBMCs destined for platelet deletion cells were processed immediately.

The total PBMCs cell preparation was first immunolabeled with magnetically-coupled antibodies against the platelet marker CD61. The 11 million platelet-depleted PBMCs were then centrifuged at 300 x g for 10 minutes. After spin, the supernatant was aspirated and cells were resuspended in 80 ul of HBSS. Then 20 ul of the CD61 MicroBeads (Miltenyi Biotec, Cat# 130-051-101) were added to the cells and incubated for 15 minutes at 4°C to magnetically label platelets. Cells were washed with 2 ml of HBSS and centrifuged at 300 x g for 10 minutes. The LS column (Miltenyi Biotec, Cat# 130-042-401) was placed in the magnetic field of the MACS Separator (Miltenyi Biotec, Cat# 130-091-051). The LS column was equilibrated with HBSS, cells resuspended in 500 ul of HBSS were applied to the LS column, and the CD61- cells were flown through the column and collected in a 15 ml collection tube. The LS column was then washed 3x with 500 ul of HBSS. The flow through was then spun at 500 x g for 10 minutes, the cell pellet was resuspended in 2 ml of HBSS and re-counted to isolate 10 M platelet-depleted cells. These cells were pelleted at 2,000 x g for 10 minutes at 4°C, the supernatant removed, and cell pellet stored at -80°C. The platelets (CD61^{+}) were recovered by flushing 1 ml of HBSS though the LS column with the plunger in a new tube, centrifuged at 3,000 x g for 10 minutes, the supernatant removed, and the cell pellet stored at -80°C until all samples could be processed for enzymatic activity assays as a single batch. For each participant, this experiment yielded three samples: 1) total PBMCs, 2) platelet depleted PBMCs, and 3) enriched platelets. Each sample was processed in parallel for RC enzymatic activity assays and mtDNAcn as described above.

Statistical analyses

To adjust for potential order effects across the 340 samples (31 samples per 96-well plate, 17 plates total) a linear adjustment was applied to raw values enzymatic activity measures, which adjusts for potential storage and batch effects, ensuring consistency between the first and last samples assayed. Samples from both the cohort and repeat participant were processed and analyzed as a single batch.

Mann-Whitney T tests were used to compare sex differences in cell type proportions and mitochondrial measures. Throughout, effect sizes between groups were computed as Hedges' g (g) to quantify the magnitude of group differences in cell type proportions and mitochondrial measures (by sex, mitotype cell subtype and inter-individual differences). Spearman's r (r) was used to assess strength of associations between continuous variables such as age and cell proportion or age and mitochondrial measures. To assess to what extent mitochondrial features are correlated across cell subtypes (co-regulation) and to calculate the average correlation across mitotypes, Spearman's r matrixes were first computed and transformed to Fisher's Z', and then averaged before transforming back to Spearman's r ($r_{z'}$). One-way non-parametric ANOVA Kruskal-Wallis with post-hoc Dunn's multiple comparison tests were used to compare cell type mitochondrial measures in different cell subtypes and PBMCs. Between- and within-person variation were characterized using coefficients of variation (C.V.). The root mean square of successive differences (rMSSD) was computed to quantify the magnitude of variability between successive weeks for repeated measures. Chi-square tests were computed to compare proportion of mitotype indices categories (enzyme activity per CS, enzyme ratios, enzyme per mtDNA, enzyme per mtDNA density, and enzyme per mtDNA relative to mtDNA density) by age (lower vs higher with increased age) and sex (lower vs higher in men). Finally, one-way non-parametric Friedman tests with post hoc Dunn's multiple comparisons were used to compare mitochondrial measures in platelet-depleted PBMCs, enriched platelets PBMCs, and total PBMCs. Statistical analyses were performed with Prism 8 (GraphPad, CA), R version 4.0.2 and RStudio version 1.3.1056. Statistical significance was set at $p<0.05$.

Data Availability

Further information and requests for resources should be directed to and will be fulfilled by the corresponding author. The raw datasets generated and analyzed in this study are available upon reasonable request.

Acknowledgements

Work of the authors is supported by the Wharton Fund and NIH grants MH119336, GM119793, MH122706, AG066828, AG056635, AG026307, and UL1TR001873. These studies used the resources of the Irving Cancer Center Core Facility funded in part through center grant P30CA013696.

Author contributions

C.T., R.G.R., K.R.K., S.H., and M.P. designed research. S.R., C.T. and A.M. recruited participants. S.R., M.A.M., and W.W. processed samples and collected data. S.R., C.T, A.J., S.C.S, R.G.R. analyzed and interpreted data. S.R. and M.P. drafted the manuscript. All authors edited and commented on the final version of the manuscript.

References

1. Picard M, Wallace DC, Burelle Y. The rise of mitochondria in medicine. *Mitochondrion* **30**, 105-116 (2016).

2. Jang JY, Blum A, Liu J, Finkel T. The role of mitochondria in aging. *The Journal of Clinical Investigation* **128**, 3662-3670 (2018).

3. Wallace Douglas C. Mitochondrial DNA Variation in Human Radiation and Disease. *Cell* **163**, 33-38 (2015).

4. Picard M, Trumpff C, Burelle Y. Mitochondrial psychobiology: foundations and applications. *Curr Opin Behav Sci* **28**, 142-151 (2019).

5. Chacko BK*, et al.* Methods for defining distinct bioenergetic profiles in platelets, lymphocytes, monocytes, and neutrophils, and the oxidative burst from human blood. *Lab Invest* **93**, 690-700 (2013).

6. Dhabhar FS, Miller AH, Stein M, McEwen BS, Spencer RL. Diurnal and Acute Stress-Induced Changes in Distribution of Peripheral Blood Leukocyte Subpopulations. *Brain, Behavior, and Immunity* **8**, 66-79 (1994).

7. Patin E*, et al.* Natural variation in the parameters of innate immune cells is preferentially driven by genetic factors. *Nature Immunology* **19**, 302-314 (2018).

8. Pyle A, Burn DJ, Gordon C, Swan C, Chinnery PF, Baudouin SV. Fall in circulating mononuclear cell mitochondrial DNA content in human sepsis. *Intensive Care Medicine* **36**, 956-962 (2010).

9. Maianski NA, Geissler J, Srinivasula SM, Alnemri ES, Roos D, Kuijpers TW. Functional characterization of mitochondria in neutrophils: a role restricted to apoptosis. *Cell Death Differ* **11**, 143-153 (2004).

10. Kramer PA, Ravi S, Chacko B, Johnson MS, Darley-Usmar VM. A review of the mitochondrial and glycolytic metabolism in human platelets and leukocytes: implications for their use as bioenergetic biomarkers. *Redox Biol* **2**, 206-210 (2014).

11. Hurtado-Roca Y*, et al.* Adjusting MtDNA Quantification in Whole Blood for Peripheral Blood Platelet and Leukocyte Counts. *PLOS ONE* **11**, e0163770 (2016).

12. Banas B, Kost BP, Goebel FD. Platelets, a typical source of error in real-time PCR quantification of mitochondrial DNA content in human peripheral blood cells. *Eur J Med Res* **9**, 371-377 (2004).

13. Urata M, Koga-Wada Y, Kayamori Y, Kang D. Platelet contamination causes large variation as well as overestimation of mitochondrial DNA content of peripheral blood mononuclear cells. *Ann Clin Biochem* **45**, 513-514 (2008).

14. Shim HB, Arshad O, Gadawska I, Côté HCF, Hsieh AYY. Platelet mtDNA content and leukocyte count influence whole blood mtDNA content. *Mitochondrion* **52**, 108-114 (2020).

15. Pagliarini DJ*, et al.* A mitochondrial protein compendium elucidates complex I disease biology. *Cell* **134**, 112-123 (2008).

16. Fecher C*, et al.* Cell-type-specific profiling of brain mitochondria reveals functional and molecular diversity. *Nature Neuroscience* **22**, 1731-1742 (2019).

17. Picard M, Hepple RT, Burelle Y. Mitochondrial functional specialization in glycolytic and oxidative muscle fibers: tailoring the organelle for optimal function. *Am J Physiol Cell Physiol* **302**, C629-641 (2012).

18. Pearce EL, Poffenberger MC, Chang C-H, Jones RG. Fueling Immunity: Insights into Metabolism and Lymphocyte Function. *Science* **342**, 1242454 (2013).

19. Nomura M*, et al.* Fatty acid oxidation in macrophage polarization. *Nature immunology* **17**, 216-217 (2016).

20. Michalek RD*, et al.* Cutting edge: distinct glycolytic and lipid oxidative metabolic programs are essential for effector and regulatory CD4+ T cell subsets. *J Immunol* **186**, 3299-3303 (2011).

21. Jones N*, et al.* Akt and STAT5 mediate naïve human CD4+ T-cell early metabolic response to TCR stimulation. *Nature Communications* **10**, 2042 (2019).

22. Brand K. Glutamine and glucose metabolism during thymocyte proliferation. Pathways of glutamine and glutamate metabolism. *Biochem J* **228**, 353-361 (1985).

23. Ron-Harel N*, et al.* T Cell Activation Depends on Extracellular Alanine. *Cell Rep* **28**, 3011-3021.e3014 (2019).

24. Bektas A*, et al.* Age-associated changes in human CD4(+) T cells point to mitochondrial dysfunction consequent to impaired autophagy. *Aging (Albany NY)* **11**, 9234-9263 (2019).

25. Picard M, McEwen BS. Psychological Stress and Mitochondria: A Systematic Review. *Psychosom Med* **80**, 141-153 (2018).

26. Gan Z, Fu T, Kelly DP, Vega RB. Skeletal muscle mitochondrial remodeling in exercise and diseases. *Cell Research* **28**, 969-980 (2018).

27. Picard M*, et al.* A Mitochondrial Health Index Sensitive to Mood and Caregiving Stress. *Biol Psychiatry* **84**, 9-17 (2018).

28. Nikolich-Žugich J. Aging of the T cell compartment in mice and humans: from no naive expectations to foggy memories. *J Immunol* **193**, 2622-2629 (2014).

29. Larsen S*, et al.* Biomarkers of mitochondrial content in skeletal muscle of healthy young human subjects. *J Physiol* **590**, 3349-3360 (2012).

30. Weiss SL*, et al.* Mitochondrial dysfunction in peripheral blood mononuclear cells in pediatric septic shock. *Pediatr Crit Care Med* **16**, e4-e12 (2015).

31. Karabatsiakis A*, et al.* Mitochondrial respiration in peripheral blood mononuclear cells correlates with depressive subsymptoms and severity of major depression. *Translational Psychiatry* **4**, e397-e397 (2014).

32. Dixon N*, et al.* Pilot study of mitochondrial bioenergetics in subjects with acute porphyrias. *Mol Genet Metab* **128**, 228-235 (2019).

33. Ehinger JK, Morota S, Hansson MJ, Paul G, Elmér E. Mitochondrial Respiratory Function in Peripheral Blood Cells from Huntington's Disease Patients. *Mov Disord Clin Pract* **3**, 472-482 (2016).

34. Tyrrell DJ, Bharadwaj MS, Van Horn CG, Marsh AP, Nicklas BJ, Molina AJ. Blood-cell bioenergetics are associated with physical function and inflammation in overweight/obese older adults. *Exp Gerontol* **70**, 84-91 (2015).

35. Butler LM*, et al.* Sequential adhesion of platelets and leukocytes from flowing whole blood onto a collagen-coated surface: requirement for a GpVI-binding site in collagen. *Thromb Haemost* **97**, 814-821 (2007).

36. Biino G*, et al.* Age- and sex-related variations in platelet count in Italy: a proposal of reference ranges based on 40987 subjects' data. *PloS one* **8**, e54289-e54289 (2013).

37. Zhang J, Li M, He Y. Large population study for age- and gender- related variations of platelet indices in Southwest China healthy adults. *Hematology & Transfusion International Journal* **1**, (2015).

38. Verhoeven JE*, et al.* Depression, telomeres and mitochondrial DNA: between- and within-person associations from a 10-year longitudinal study. *Mol Psychiatry* **23**, 850-857 (2018).

39. Mengel-From J, Thinggaard M, Dalgård C, Kyvik KO, Christensen K, Christiansen L. Mitochondrial DNA copy number in peripheral blood cells declines with age and is associated with general health among elderly. *Hum Genet* **133**, 1149-1159 (2014).

40. Zhang R, Wang Y, Ye K, Picard M, Gu Z. Independent impacts of aging on mitochondrial DNA quantity and quality in humans. *BMC Genomics* **18**, 890 (2017).

41. Nicoli F*, et al.* Naïve CD8+ T-Cells Engage a Versatile Metabolic Program Upon Activation in Humans and Differ Energetically From Memory CD8+ T-Cells. *Frontiers in Immunology* **9**, (2018).

42. van der Windt GJW*, et al.* CD8 memory T cells have a bioenergetic advantage that underlies their rapid recall ability. *Proceedings of the National Academy of Sciences* **110**, 14336 (2013).

43. Ackermann K, Revell VL, Lao O, Rombouts EJ, Skene DJ, Kayser M. Diurnal rhythms in blood cell populations and the effect of acute sleep deprivation in healthy young men. *Sleep* **35**, 933-940 (2012).

44. Dhabhar FS, Malarkey WB, Neri E, McEwen BS. Stress-induced redistribution of immune cells--from barracks to boulevards to battlefields: a tale of three hormones--Curt Richter Award winner. *Psychoneuroendocrinology* **37**, 1345-1368 (2012).

45. Beis D*, et al.* The Role of Norepinephrine and α-Adrenergic Receptors in Acute Stress-Induced Changes in Granulocytes and Monocytes. *Psychosom Med* **80**, 649-658 (2018).

46. Chacko BK, Zhi D, Darley-Usmar VM, Mitchell T. The Bioenergetic Health Index is a sensitive measure of oxidative stress in human monocytes. *Redox Biol* **8**, 43-50 (2016).

47. Picard M*, et al.* Mitochondrial dysfunction and lipid accumulation in the human diaphragm during mechanical ventilation. *Am J Respir Crit Care Med* **186**, 1140-1149 (2012).

48. Calvo SE, Clauser KR, Mootha VK. MitoCarta2.0: an updated inventory of mammalian mitochondrial proteins. *Nucleic Acids Res* **44**, D1251-1257 (2016).

49. van der Windt GJ*, et al.* Mitochondrial respiratory capacity is a critical regulator of CD8+ T cell memory development. *Immunity* **36**, 68-78 (2012).

50. Iershov A*, et al.* The class 3 PI3K coordinates autophagy and mitochondrial lipid catabolism by controlling nuclear receptor PPARα. *Nature Communications* **10**, 1566 (2019).

51. Turner N*, et al.* Excess lipid availability increases mitochondrial fatty acid oxidative capacity in muscle: evidence against a role for reduced fatty acid oxidation in lipid-induced insulin resistance in rodents. *Diabetes* **56**, 2085-2092 (2007).

52. Lindquist C, Bjørndal B, Rossmann CR, Svardal A, Hallström S, Berge RK. A fatty acid analogue targeting mitochondria exerts a plasma triacylglycerol lowering effect in rats with impaired carnitine biosynthesis. *PLoS One* **13**, e0194978 (2018).

53. Karan KR*, et al.* Mitochondrial respiratory capacity modulates LPS-induced inflammatory signatures in human blood. *Brain, Behavior, & Immunity - Health* **5**, 100080 (2020).

54. Artyomov MN, Van den Bossche J. Immunometabolism in the Single-Cell Era. *Cell Metabolism*, (2020).

55. Segerstrom SC, Sephton SE, Westgate PM. Intraindividual variability in cortisol: Approaches, illustrations, and recommendations. *Psychoneuroendocrinology* **78**, 114-124 (2017).

56. Ventura-Clapier R, Piquereau J, Veksler V, Garnier A. Estrogens, Estrogen Receptors Effects on Cardiac and Skeletal Muscle Mitochondria. *Frontiers in Endocrinology* **10**, (2019).

57. Silaidos C*, et al.* Sex-associated differences in mitochondrial function in human peripheral blood mononuclear cells (PBMCs) and brain. *Biology of Sex Differences* **9**, 34 (2018).

58. Short KR*, et al.* Decline in skeletal muscle mitochondrial function with aging in humans. *Proc Natl Acad Sci U S A* **102**, 5618-5623 (2005).

59. Hebert SL*, et al.* Mitochondrial Aging and Physical Decline: Insights From Three Generations of Women. *J Gerontol A Biol Sci Med Sci* **70**, 1409-1417 (2015).

60. Wachsmuth M, Hübner A, Li M, Madea B, Stoneking M. Age-Related and Heteroplasmy-Related Variation in Human mtDNA Copy Number. *PLOS Genetics* **12**, e1005939 (2016).

61. Moore AZ*, et al.* Influence of cell distribution and diabetes status on the association between mitochondrial DNA copy number and aging phenotypes in the InCHIANTI study. *Aging Cell* **17**, e12683 (2018).

62. Ye K, Lu J, Ma F, Keinan A, Gu Z. Extensive pathogenicity of mitochondrial heteroplasmy in healthy human individuals. *Proceedings of the National Academy of Sciences* **111**, 10654 (2014).

63. Giordano C*, et al.* Efficient mitochondrial biogenesis drives incomplete penetrance in Leber's hereditary optic neuropathy. *Brain* **137**, 335-353 (2014).

64. Yu-Wai-Man P*, et al.* OPA1 mutations cause cytochrome c oxidase deficiency due to loss of wild-type mtDNA molecules. *Hum Mol Genet* **19**, 3043-3052 (2010).

Figure Legends

Figure 1 – Immune cell subtype distribution in adult women and men.

(**a**) Overview of participant demographics, blood collection, processing, and analysis pipeline. Total leukocytes were isolated using Ficoll 1119 and PBMCs were isolated on Ficoll 1077. The five mitochondrial features analyzed on the mitochondrial phenotyping platform are colored. (**b**) Stacked histogram showing the leukocytes distribution derived from the complete blood count (CBC). (**c**) Diagram illustrating the proportion of circulating immune cell subtypes (% of all detected cells) quantified by flow cytometry from total peripheral blood leukocytes. Cell surface markers and subtype definitions are detailed in Supplemental Table 1. (**d**) Forest plot of the effect sizes for cell subtype distribution differences between women (n=11) and men (n=10). P-values from non-parametric Mann-Whitney T test. The fold change comparing raw counts between women and men and shown on the right. Error bars reflect the 95% confidence interval (C.I.) on the effect size. (**e**) Distribution of cell types proportions in women and men illustrating the range of $CD4^+$ and $CD8^+$ naïve cells, B cells, and monocytes, highlighting the natural variation among our cohort. Each datapoint reflects a different individual. (**f**) Spearman's r correlation between age and cell types proportion. n=21, $p<0.05$*, $p<0.01$**.

Figure 2 – Influence of cell subtypes on mitochondrial features in total PBMCs.

(**a**) Pairwise correlations of cell subtype proportions obtained from cell sorting with mitochondrial features measured in PBMCs for the cohort (n=20). Aggregate correlations are shown as a heatmap (top) and (**b**) individual scatterplots (bottom).

Figure 3 – Influence of platelet contamination on mitochondrial features in total PBMCs.

(**a**) Schematic of the natural state of Ficoll-isolated PBMCs associated with contaminating platelets. (**b**) Association of age and circulating platelet abundance (i.e., count) in our cohort (Spearman's r). (**c**) Change in platelet abundance as a function of age. The magnitude of the association (slope of the regression: 109 platelets/L per year) from two large epidemiological studies and our cohort. The inset shows the actual regressions (n=21 to 22,351). (**d**) Effect sizes of the association between platelet count and PBMCs mitochondrial features in our cohort (n=20). (**e**) Overview of the experimental PBMC platelet depletion study, yielding three different samples subjected to mitochondrial phenotyping. (**f**) Fold change in mitochondrial parameters between i) platelet-depleted PBMCs and ii) enriched platelets (with contaminating PBMCs) relative iii) total PBMCs. P-values from One-Way non-parametric ANOVA Friedman test, post-hoc Dunn's

multiple comparisons relative to total PBMCs. (**g**) Percent change of platelet-depleted PBMCs mitochondrial features from total PBMCs. n=9, p<0.05*, p<0.01**, p<0.001***, p<0.0001****.

Figure 4 – Cell subtype differences in mitochondrial content and RC function.
(**a-e**) Violin plots illustrating immune cell type differences in mitochondrial features across cell subtypes and total PBMCs. For each individual, only the 6 most abundant cell types were analyzed (n=21 individuals, 12-18 per cell subtype). Dashed lines are median (thick) and 25th and 75th quartiles (thin). P-values from One-Way non-parametric ANOVA Kruskal-Wallis test, post-hoc Dunn's multiple comparisons relative to PBMCs. (**f**) Spearman's r inter-correlations of mitochondrial features across subtypes. Insets show the scatterplots for selected correlations. p<0.05*, p<0.01**, p<0.001***, p<0.0001****.

Figure 5 – Mitochondrial health index (MHI) and coherence of mitochondrial features across cell subtypes.
(**a**) Schematic of the MHI equation reflecting respiratory chain function as the numerator, and markers of mitochondrial content as the denominator, producing a metric of energy production capacity on a per-mitochondrion basis. (**b**) MHI across immune cell subtypes. Dashed lines are median (thick) and 25th and 75th quartiles (thin). P-values from One-Way non-parametric ANOVA Kruskal-Wallis test with Dunn's multiple comparison test of subtypes relative to PBMCs, n=12-18 per cell subtype. (**c**) Correlation matrices showing the association between cell subtypes in mitochondrial features. Correlations were not computed for cell subtype pairs with fewer than n=6 observations (gray cell). (**d**) Average effect sizes reflecting the within-person coherence of mitochondrial features across cell types (calculated using Fisher z-transformation). p<0.05*, p<0.001***.

Figure 6 – Associations of mitochondrial features with sex and age across cell subtypes.
(**a-f**) Effect size of sex differences in mitochondrial activity across cell subtypes quantified by Hedges' g. The fold change computed from raw values is shown on the right. P-values from Mann-Whitney test. Error bars reflect the 95% C.I. on the effect size. (**g-l**) Association of age and mitochondrial features across cell subtypes. P-values from Spearman's r correlations, not adjusted for multiple comparisons. n=21 (11 women, 10 men), p<0.05*, p<0.01**, p<0.001***.

Figure 7 – Within-person variability of mitochondrial features across cell subtypes.
(**a**) Overview of the repeat participant design, including blood collection, processing, and analysis. All samples were collected, stored, and processed as a single batch with samples from the cohort. (**b-g**) Natural weekly variation for each mitochondrial feature across cell subtypes in the same

person across 9 weeks represented as scaled centered data where 1 unit change represents a one-standard deviation (S.D.) difference. Root mean square of the successive differences (rMSSDs) quantify the magnitude of variability between successive weeks. The coefficients of variation (C.V.) quantify the magnitude of variability across the total 9 weeks. Monocytes and CD4+ CM-EM were not collected on weeks 1 and 2. (**h**) Side-by-side comparison of CS activity between the cohort (n=12-18 per cell subtype) and the repeat participant (n=7-9 time points) across cell subtypes. The dynamic range of two cell subtypes are represented: monocytes and CD4+ naïve T cells. (**i**) Within-person correlation matrices between cell subtypes for each mitochondrial feature over 9 weeks, illustrating to what extent cell subtypes are correlated with each other (co-regulation). (**j**) Average inter-correlation across all cell subtypes by mitochondrial feature (calculated using Fisher z-transformation) indicating the degree of coherence within person. (**k**) Comparison of co-regulation patterns among mitochondrial features between the cohort and the repeat participant. Each datapoint represents a cell subtype pair.

Figure 8 – Mitotypes in purified leukocyte populations from the cohort and repeated-measures.

(**a**) Schematic illustrating the multivariate approach to generate and visualize mitotypes by putting into relation two or more mitochondrial features. Notice the similarity and added insight relative to single metrics, similar to the integration of height and weight into body mass index (BMI). (**b-e**) Mitotypes plotted for each cell subtype among the cohort. Data are means and SEM. Overlaid shaded areas denote general leukocyte categories. (**f**) Summary of mitotype differences between (i) innate and adaptive subdivisions and (ii) naïve and memory T cells. (**g-i**) Validation of subtype-specific mitotype differences in the repeat participant, illustrating the conserved nature of mitotypes across individuals. Only the six cell subtypes analyzed in the repeat participant are plotted. (**j**) Comparison of the magnitude of the difference (Hedges' g) in mitotypes between cell types, and between individuals. Dark blue bars indicate the magnitude of the dominant difference in mitotypes between cell subtypes. Light blue bars indicate the magnitude of the difference in mitotypes between the cohort and the repeat participant within a cell type. Error bars reflect the 95% C.I. on the effect size.

Figure 9 – Mitotype distribution and strength of difference across sex and age.

(**a**) Ranking of mitotype indices by their difference between women and men, quantified as the effect size (Hedges' g) between women and men. A total of 16 mitotype indices were generated, subdivided into 5 main color-coded categories (see Supplemental Figure 7). Pie charts illustrate the proportion mitotypes belonging to each category that are either higher in women (left) or in

men (right). P-values for enrichment of sexually dimorphic mitotypes are derived from Chi-square test. (**b**) Violin plots illustrating the two mitotypes with the largest opposite sex differences, both showing large effect sizes (g). (**c**) Heatmap of sex differences (Hedges' g) for primary measures of mitochondrial function (top) and multivariate mitotypes (bottom) across cell subtypes. The histogram at the bottom shows the average absolute effect size across all mitotypes (calculated from absolute values). (**d**) Ranking of mitotype indices by the strength and direction of their association with age, with enrichment analysis analyzed as for sex (Chi-square test). (**e**) Spearman's r correlations of mitotypes/cell type combinations with the strongest positive and negative associations with age. (**f**) Heatmap of the age correlations (Spearman's r) for primary features and composite mitotypes across cell subtypes. The histogram at the bottom shows the average effect size (r) for each cell subtype (calculated using absolute values and Fisher z-transformation). $p<0.05$*, $p<0.01$**, $p<0.001$***, $p<0.0001$****.

Figure 10 – Association of blood biomarkers with mitochondrial parameters across cell subtypes and primary mitochondrial features.

(**a**) Overview of blood biochemistry, hormonal, and metabolic biomarkers collected for each participant. (**b**) Sex- and age-adjusted correlations between blood biomarkers and mitochondrial features across cell subtypes for the cohort (n=10-20 per mito-biomarker combinations) shown as a heatmap. (**c**) Same as (b) but using repeated-measures of mitochondrial features and biomarkers in the repeat participant. (**d**) Scatterplots of the indicated correlations between Neutrophils CS activity and LDL cholesterol (left), and CD4+ CM-EM mtDNAcn and potassium (K+) (right) for the cohort (top row) and the repeat participant (bottom row). (**e**) Frequency distributions of the aggregated effect sizes between biomarkers and mitochondrial features across cell subtypes for the cohort (total correlation pairs=1,080) and the repeat participant (total correlation pairs=882).

SUPPLEMENTAL MATERIAL

Supplemental Figure 1 – Diagram of leukocyte cell lineages.

Cells analyzed in this study are circled in red. The cell surface markers used to define sub-populations are indicated below each cell subtype. Diagram adapted from: https://oerpub.github.io/epubjs-demo-book/content/m46036.xhtml#fig-ch03_06_01.

Supplemental Figure 2 – Gating strategy to quantify all cell subtypes and sorting major cell subtypes for mitochondrial phenotyping.

See the methods section for details of labeling cocktails and cell sorter parameters. An initial run of 2M cells was used to establish the six most abundant cell subtypes (targets) for each participant, followed by FACS to obtain at least one 5M aliquot of each target cell subtype. Up to five 5M aliquots were collected per cell subtype, per participant, to establish technical variability in downstream assays.

Supplemental Figure 3 – Sex differences and age correlations with leukocyte abundance measured by complete blood count.

(**a**) Forest plot illustrating the effect size (g) of the sex differences in cell proportion derived from the complete blood count (CBC) results (n=21). Fold changes in the raw values are also shown. P-values from non-parametric Mann-Whitney T test. Error bars reflect the 95% C.I. on the effect size. (**b**) Correlation (Spearman's r) between age and cell proportion derived from the complete blood count. n=21, $p<0.05$*.

Supplemental Figure 4 – Associations between CBC cell proportions and subtype-specific enzymatic activities with mitochondrial features measured in PBMCs.

(**a**) Correlations between CBC-based cell type abundance (% of total leukocytes) and PBMCs mitochondrial features for the cohort (n=20). (**b**) Correlations of the mitochondrial features measured in each cell subtype and the same mitochondrial feature measured in PBMCs for the cohort (n=12-20). Heatmaps for the cohort show to what extent PBMCs-based measures reflect activities in various immunologically-defined cell subtypes. This data integrates data presented in Figure 5, here focused on PBMCs.

Supplemental Figure 5 – Association between age and cell subtype mitochondrial features.

(**a-i**) Correlations between mitochondria features and age. This figure presents the same data as main Figure 4, but organized by cell subtypes rather than mitochondrial feature to facilitate the visualization of subtype-level effects. Spearman's r, $p<0.05$*, $p<0.01$**, $p<0.001$***.

Supplemental Figure 6 – Within-person variability of cell subtype proportions overtime.

(**a**) Within-person variation of cell type proportions across 9 weeks. The FACS-derived raw cell proportions (% of total cells) are shown on the left. Root mean square of successive differences (rMSSD) illustrating the magnitude of variability between successive weeks, and C.V. illustrating the magnitude of variability across the total 9 weeks are provided on the right for each cell subtype, by mitochondrial feature. (**b**) Same as a, but based on CBC results.

Supplemental Figure 7 – Associations between subtype-specific and CBC cell proportions, and subtype-specific enzymatic activities with mitochondrial features measured in PBMCs.

(**a**) Pairwise correlations of cell subtype proportions obtained from cell sorting with mitochondrial features measured in PBMCs for the repeat participant (n=1 x 9 timepoints). Aggregate correlations are shown as a heatmap (top) and individual scatterplots (bottom). (**b**) Frequency distributions of the effect sizes between PBMC mitochondrial features and cell subtypes proportions for the cohort (Figure 2) and the repeat participant (total correlation pairs=72, for both). (**c**) Correlations between CBC-based cell type abundance (% of total leukocytes) and PBMCs mitochondrial features for the repeat participant (n=1 x 9 timepoints). (**d**) Frequency distribution of effect sizes. (**e**) Correlations of the mitochondrial features measured in each cell subtype and the same mitochondrial feature measured in PBMCs for the repeat participant. Heatmaps for the repeat participant (n=1 x 9 timepoints) show to what extent PBMCs-based measures reflect activities in various immunologically-defined cell subtypes. This data integrates data presented in Figure 7, here focused on PBMCs. (**f**) Frequency distributions of effect sizes for association between PBMC and cell subtype mitochondrial features for the cohort and the repeat participant (total correlation pairs=36, for both), showing a predominance of positive correlations.

Supplemental Figure 8 – Variability of mitochondrial features across cell subtypes between the cohort and the repeat participant.

(**a-e**) Side-by-side comparison of mitochondrial features between the cohort (n=12-18 per cell type) and the repeat participant (n=1 x 9 timepoints) across cell subtypes. This figure shows the same data as in main Figure 5h, but for all mitochondrial features. (**f**) Summary of a-e illustrated by a bar graph showing observed variation (C.V.) of mitochondrial features between the cohort and the repeat participant. The technical variation established on a subset of samples and likely represents a conservative overestimation of noise is shown by red lines.

Supplemental Figure 9 – Operationalization and categorization of mitotypes.

Chart illustrating mitotype ratios and their simple interpretations.

Supplemental Table 1 – Leukocyte subtypes included in the study.

Immune cell subtypes included in this study, including a brief summary of their functions and cell surface markers used for immunolabeling and FACS.

Additional references to Supplemental Table 1:

Chiu, S. and A. Bharat (2016). "Role of monocytes and macrophages in regulating immune response following lung transplantation." Current opinion in organ transplantation 21(3): 239-245.

Gasper, D. J., M. M. Tejera and M. Suresh (2014). "CD4 T-cell memory generation and maintenance." Critical reviews in immunology 34(2): 121-146.

Hoffman, W., F. G. Lakkis and G. Chalasani (2016). "B Cells, Antibodies, and More." Clinical journal of the American Society of Nephrology : CJASN 11(1): 137-154.

Luckheeram, R. V., R. Zhou, A. D. Verma and B. Xia (2012). "CD4^{+}T cells: differentiation and functions." Clinical & developmental immunology 2012: 925135-925135.

Mahnke, Y. D., T. M. Brodie, F. Sallusto, M. Roederer and E. Lugli (2013). "The who's who of T-cell differentiation: Human memory T-cell subsets." European Journal of Immunology 43(11): 2797-2809.

Martin, M. D. and V. P. Badovinac (2018). "Defining Memory CD8 T Cell." Frontiers in Immunology 9(2692).

Mayadas, T. N., X. Cullere and C. A. Lowell (2014). "The Multifaceted Functions of Neutrophils." Annual Review of Pathology: Mechanisms of Disease 9(1): 181-218.

Stubbe, M., N. Vanderheyde, M. Goldman and A. Marchant (2006). "Antigen-specific central memory CD4+ T lymphocytes produce multiple cytokines and proliferate in vivo in humans." J Immunol **177**(11): 8185-8190.

Tian, Y., M. Babor, J. Lane, V. Schulten, V. S. Patil, G. Seumois, S. L. Rosales, Z. Fu, G. Picarda, J. Burel, J. Zapardiel-Gonzalo, R. N. Tennekoon, A. D. De Silva, S. Premawansa, G. Premawansa, A. Wijewickrama, J. A. Greenbaum, P. Vijayanand, D. Weiskopf, A. Sette and B. Peters (2017). "Unique phenotypes and clonal expansions of human CD4 effector memory T cells re-expressing CD45RA." Nature Communications 8(1): 1473.

Vivier, E., E. Tomasello, M. Baratin, T. Walzer and S. Ugolini (2008). "Functions of natural killer cells." Nature Immunology 9: 503-510.

Zhang, N. and M. J. Bevan (2011). "CD8(+) T cells: foot soldiers of the immune system." Immunity 35(2): 161-168.

Supplemental Table 2 – CBC- and FACS-based cell proportions for all study participants and time points.

Participants are ordered by age. CBC measurements were performed using a Sysmex XN-9000™ instrument, and FACS-based cell proportions were determined using a BD™ Influx cell sorter. (See methods for details).

Supplemental Table 3 – Technical variation for each mitochondrial assay and calculated MHI by cell type.

Coefficients of variation (C.V.s) across 2-5 biological replicates (different 5M cell pellet isolated from the same blood draw) for each cell subtype and PBMCs (See *Methods* for details).

Supplemental Table 4 – Recipes for antibody cocktails used to detect cell surface markers for FACS-based cell proportions and sorting.
(See *Methods* for details).

Figure 1

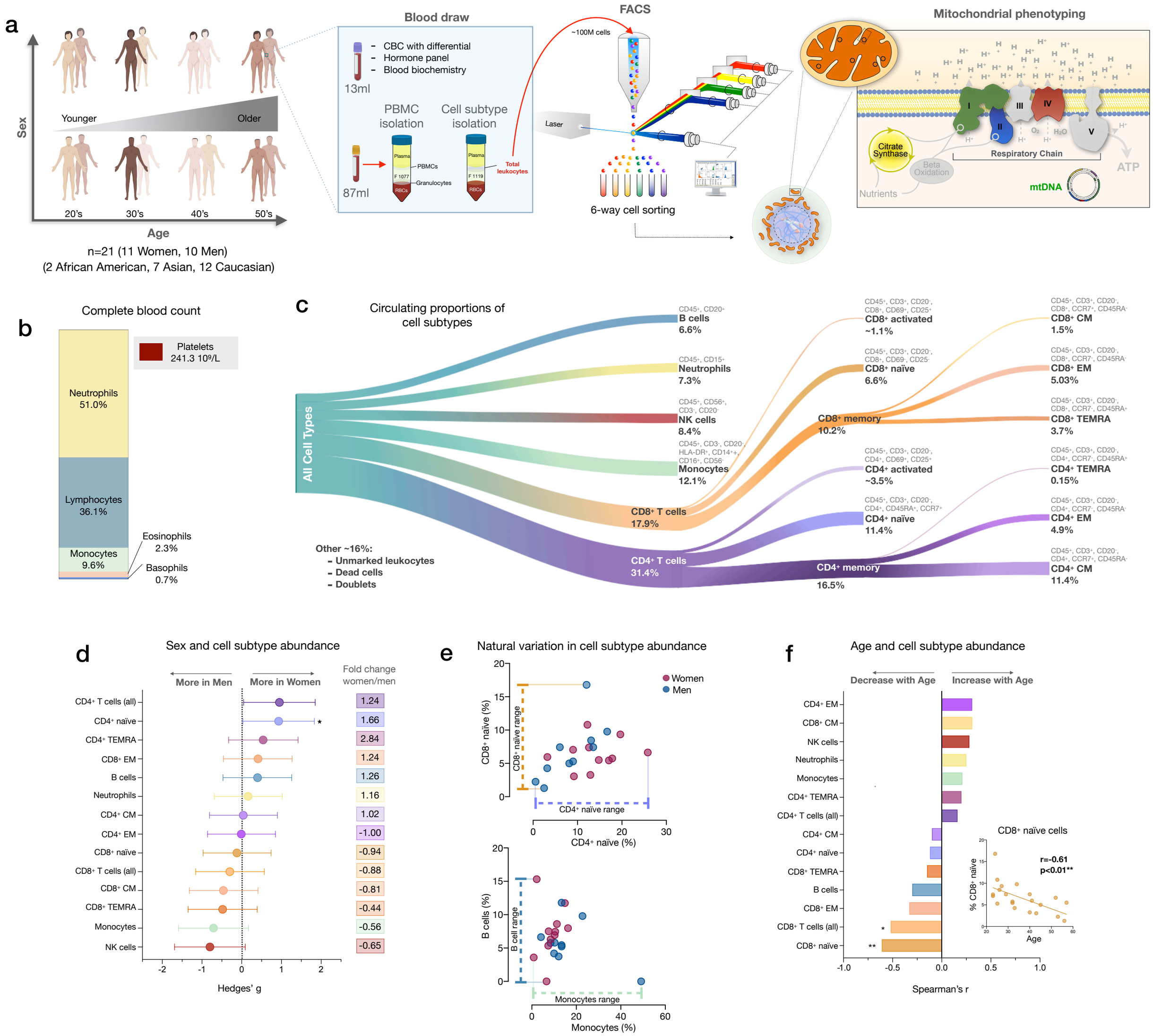

Figure 1 – Immune cell subtype distribution in adult women and men.

(**a**) Overview of participant demographics, blood collection, processing, and analysis pipeline. Total leukocytes were isolated using Ficoll 1119 and PBMCs were isolated on Ficoll 1077. The five mitochondrial features analyzed on the mitochondrial phenotyping platform are colored. (**b**) Stacked histogram showing the leukocytes distribution derived from the complete blood count (CBC). (**c**) Diagram illustrating the proportion of circulating immune cell subtypes (% of all detected cells) quantified by flow cytometry from total peripheral blood leukocytes. Cell surface markers and subtype definitions are detailed in Supplemental Table 1. (**d**) Forest plot of the effect sizes for cell subtype distribution differences between women (n=11) and men (n=10). P-values from non-parametric Mann-Whitney T test. The fold change comparing raw counts between women and men and shown on the right. Error bars reflect the 95% confidence interval (C.I.) on the effect size. (**e**) Distribution of cell types proportions in women and men illustrating the range of CD4+ and CD8+ naïve cells, B cells, and monocytes, highlighting the natural variation among our cohort. Each datapoint reflects a different individual. (**f**) Spearman's r correlation between age and cell types proportion. n=21, $p<0.05$*, $p<0.01$**.

Figure 2

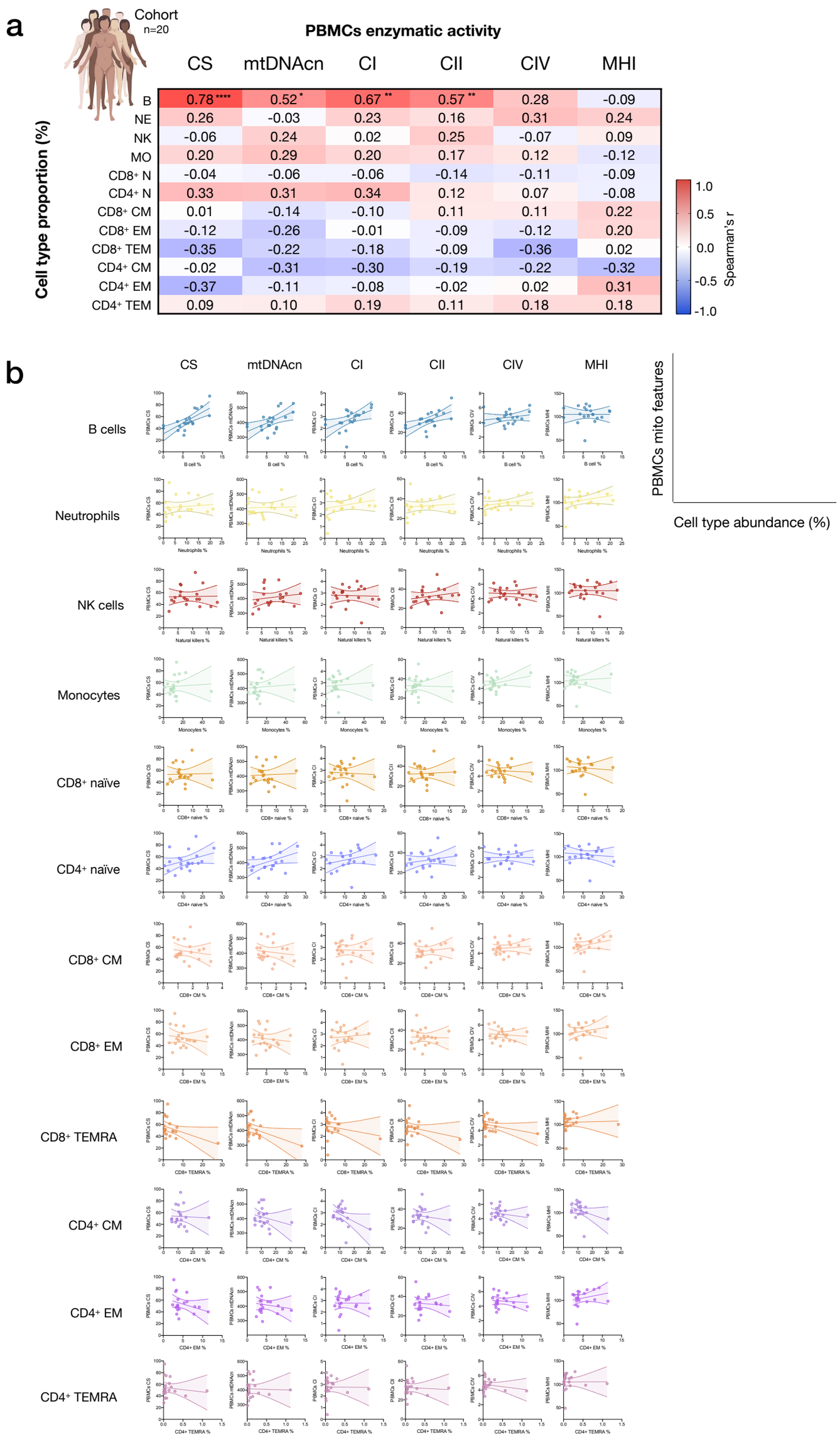

Figure 2 – Influence of cell subtypes on mitochondrial features in total PBMCs.

(**a**) Pairwise correlations of cell subtype proportions obtained from cell sorting with mitochondrial features measured in PBMCs for the cohort (n=20). Aggregate correlations are shown as a heatmap (top) and (**b**) individual scatterplots (bottom).

Figure 3

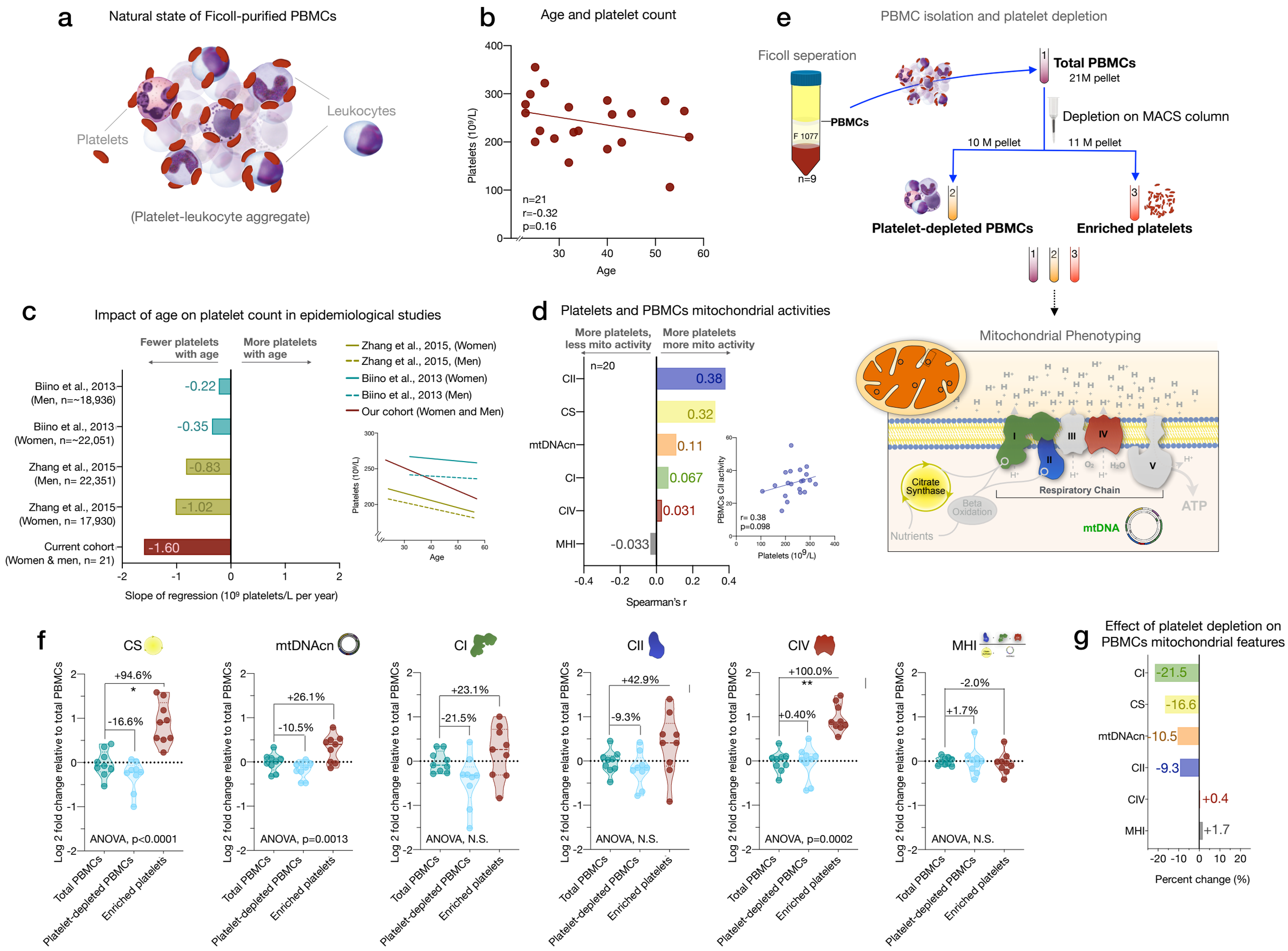

Figure 3 – Influence of platelet contamination on mitochondrial features in total PBMCs.

(**a**) Schematic of the natural state of Ficoll-isolated PBMCs associated with contaminating platelets. (**b**) Association of age and circulating platelet abundance (i.e., count) in our cohort (Spearman's r). (**c**) Change in platelet abundance as a function of age. The magnitude of the association (slope of the regression: 10^9 platelets/L per year) from two large epidemiological studies and our cohort. The inset shows the actual regressions (n=21 to 22,351). (**d**) Effect sizes of the association between platelet count and PBMCs mitochondrial features in our cohort (n=20). (**e**) Overview of the experimental PBMC platelet depletion study, yielding three different samples subjected to mitochondrial phenotyping. (**f**) Fold change in mitochondrial parameters between i) platelet-depleted PBMCs and ii) enriched platelets (with contaminating PBMCs) relative iii) total PBMCs. P-values from One-Way non-parametric ANOVA Friedman test, post-hoc Dunn's multiple comparisons relative to total PBMCs. (**g**) Percent change of platelet-depleted PBMCs mitochondrial features from total PBMCs. n=9, $p<0.05$*, $p<0.01$**, $p<0.001$***, $p<0.0001$****.

Figure 4

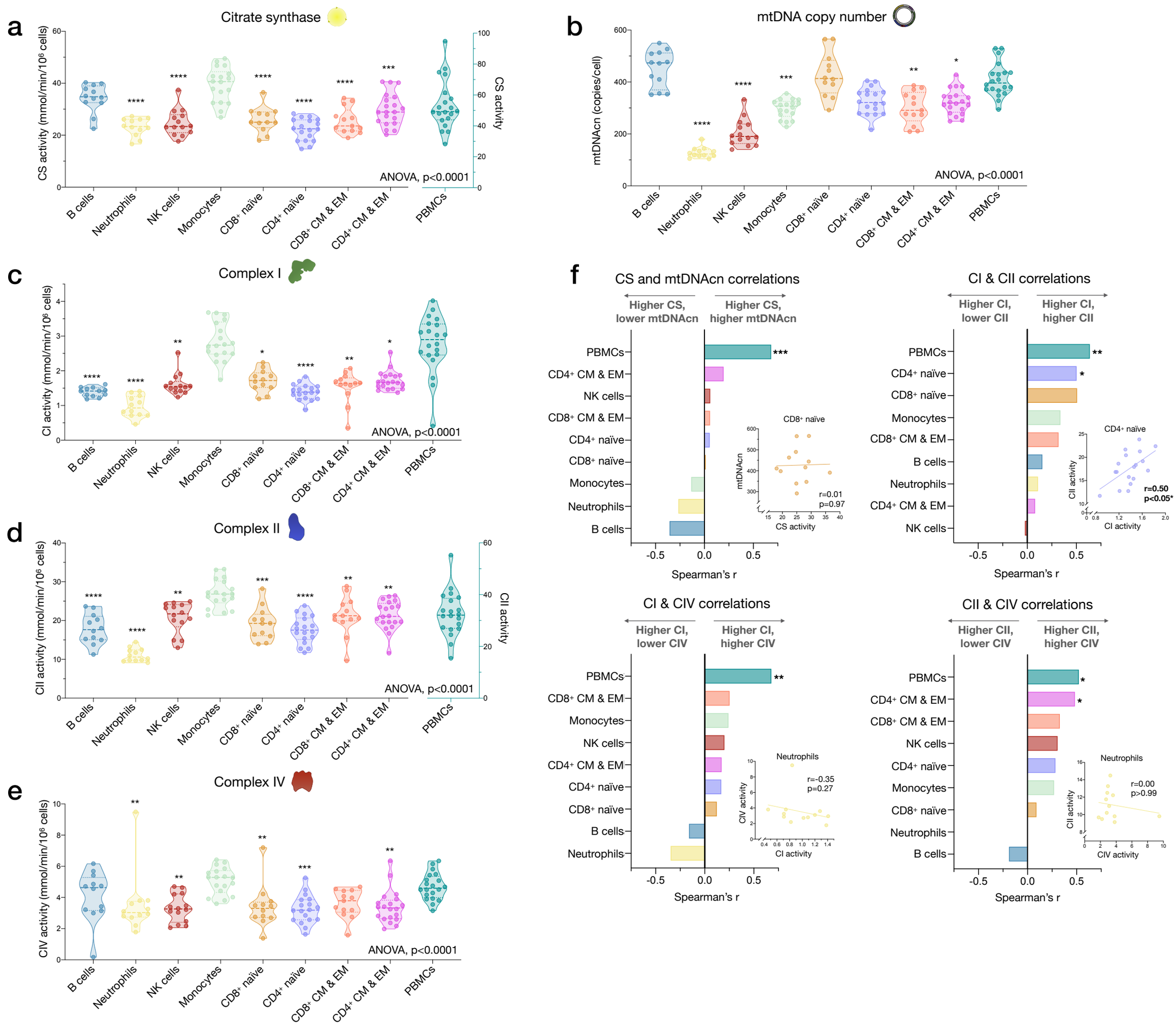

Figure 4 – Cell subtype differences in mitochondrial content and RC function.

(**a-e**) Violin plots illustrating immune cell type differences in mitochondrial features across cell subtypes and total PBMCs. For each individual, only the 6 most abundant cell types were analyzed (n=21 individuals, 12-18 per cell subtype). Dashed lines are median (thick) and 25th and 75th quartiles (thin). P-values from One-Way non-parametric ANOVA Kruskal-Wallis test, post-hoc Dunn's multiple comparisons relative to PBMCs. (**f**) Spearman's r inter-correlations of mitochondrial features across subtypes. Insets show the scatterplots for selected correlations. p<0.05*, p<0.01**, p<0.001***, p<0.0001****.

Figure 5

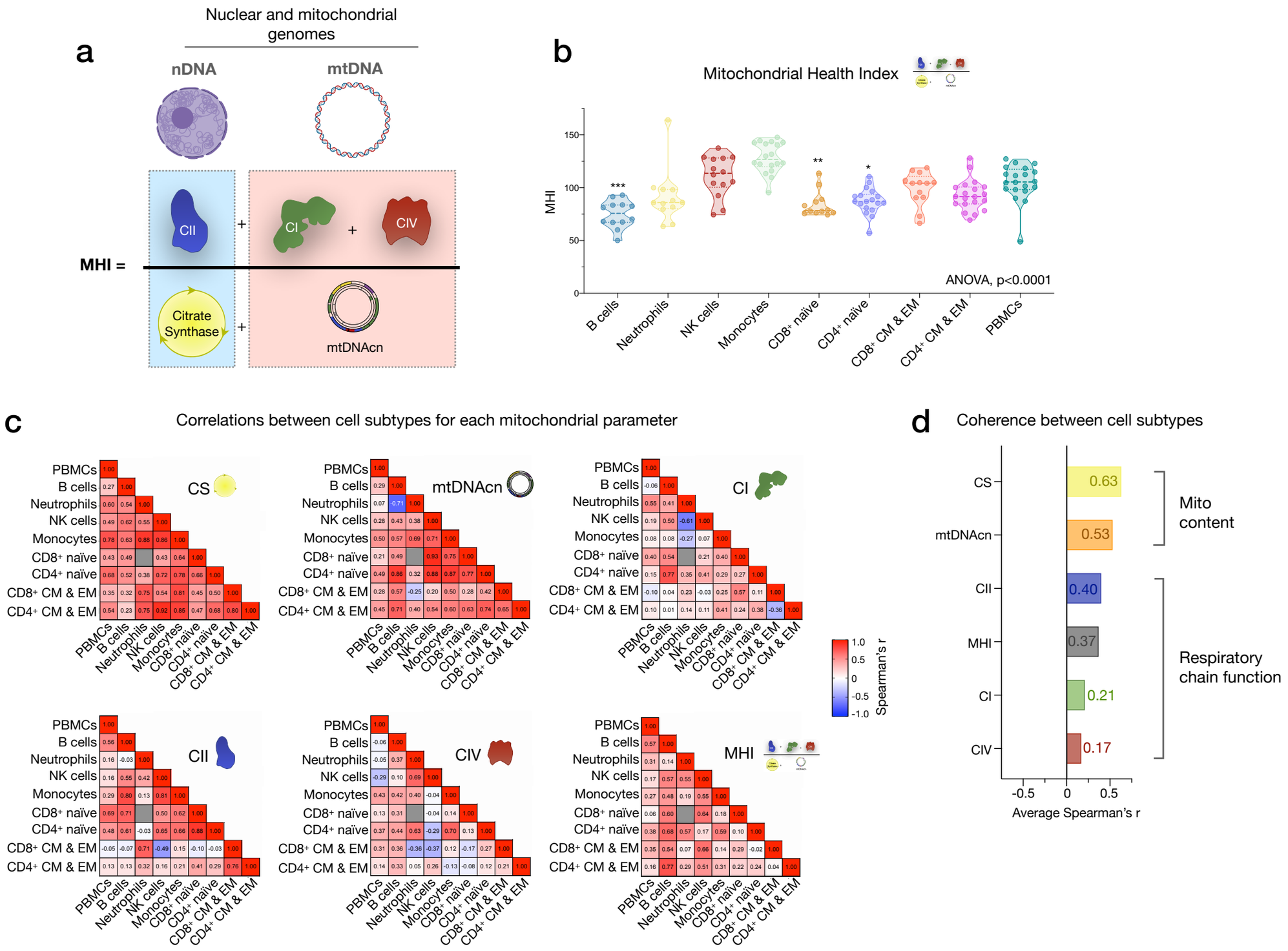

Figure 5 – Mitochondrial health index (MHI) and coherence of mitochondrial features across cell subtypes.
(**a**) Schematic of the MHI equation reflecting respiratory chain function as the numerator, and markers of mitochondrial content as the denominator, producing a metric of energy production capacity on a per-mitochondrion basis. (**b**) MHI across immune cell subtypes. Dashed lines are median (thick) and 25th and 75th quartiles (thin). P-values from One-Way non-parametric ANOVA Kruskal-Wallis test with Dunn's multiple comparison test of subtypes relative to PBMCs, n=12-18 per cell subtype. (**c**) Correlation matrices showing the association between cell subtypes in mitochondrial features. Correlations were not computed for cell subtype pairs with fewer than n=6 observations (gray cell). (**d**) Average effect sizes reflecting the within-person coherence of mitochondrial features across cell types (calculated using Fisher z-transformation). $p<0.05$*, $p<0.001$***.

Figure 6

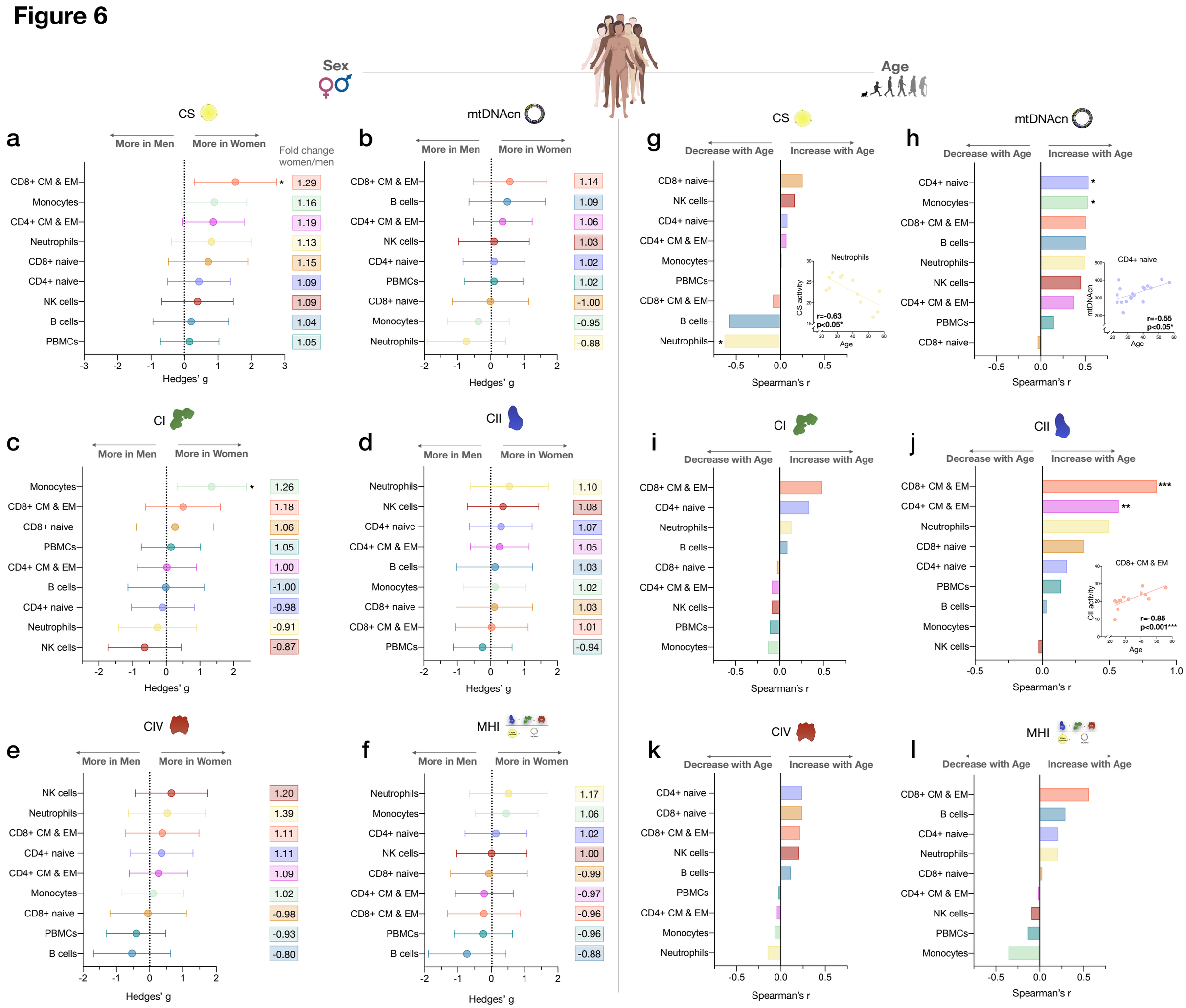

Figure 6 – Associations of mitochondrial features with sex and age across cell subtypes.

(**a-f**) Effect size of sex differences in mitochondrial activity across cell subtypes quantified by Hedges' g. The fold change computed from raw values is shown on the right. P-values from Mann-Whitney test. Error bars reflect the 95% C.I. on the effect size. (**g-l**) Association of age and mitochondrial features across cell subtypes. P-values from Spearman's r correlations, not adjusted for multiple comparisons. n=21 (11 women, 10 men), p<0.05*, p<0.01**, p<0.001***.

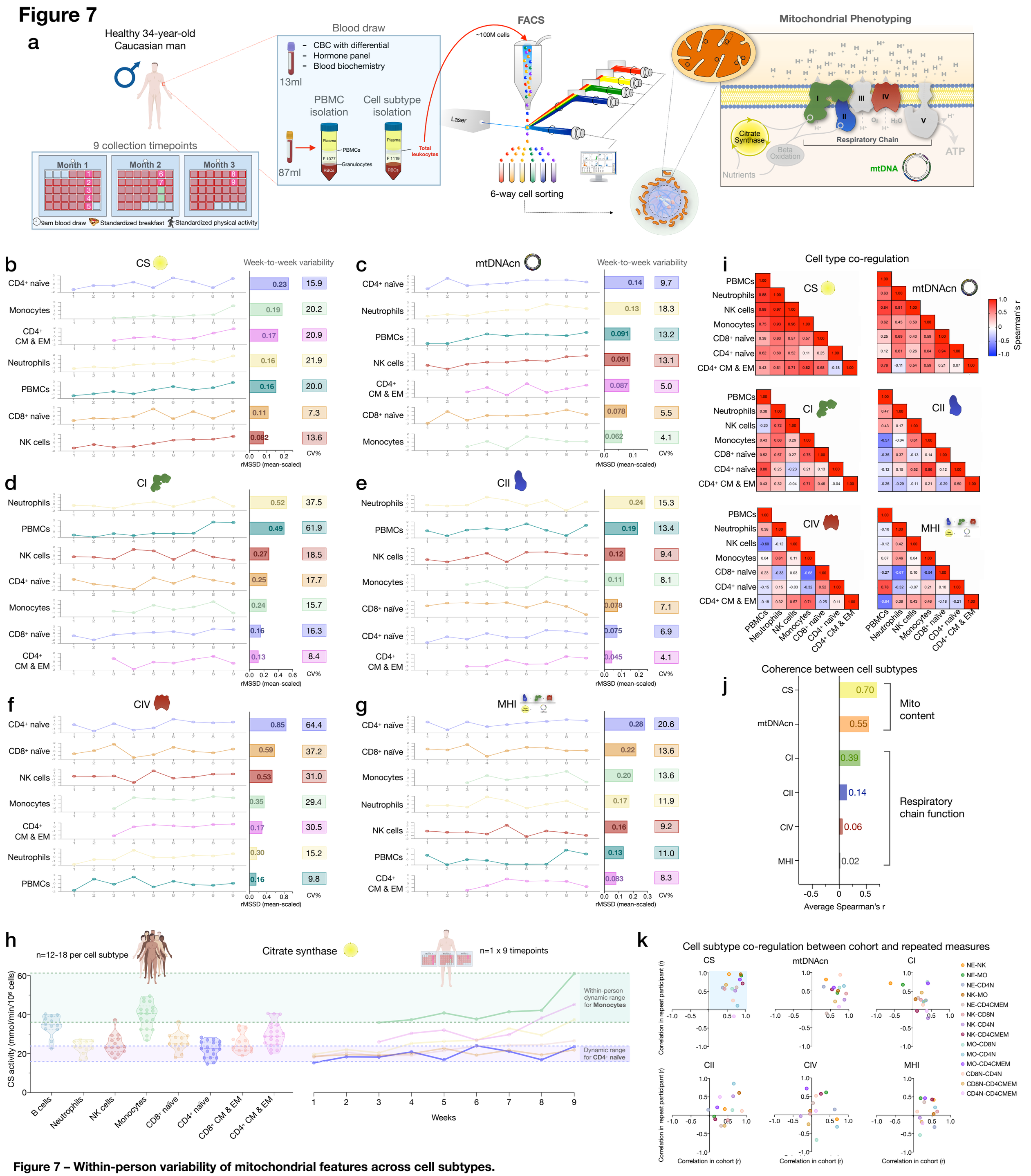

Figure 7 – Within-person variability of mitochondrial features across cell subtypes.

(**a**) Overview of the repeat participant design, including blood collection, processing, and analysis. All samples were collected, stored, and processed as a single batch with samples from the cohort. (**b-g**) Natural weekly variation for each mitochondrial feature across cell subtypes in the same person across 9 weeks represented as scaled centered data where 1 unit change represents a one-standard deviation (S.D.) difference. Root mean square of the successive differences (rMSSDs) quantify the magnitude of variability between successive weeks. The coefficients of variation (C.V.) quantify the magnitude of variability across the total 9 weeks. Monocytes and CD4+ CM-EM were not collected on weeks 1 and 2. (**h**) Side-by-side comparison of CS activity between the cohort (n=12-18 per cell subtype) and the repeat participant (n=7-9 time points) across cell subtypes. The dynamic range of two cell subtypes are represented: monocytes and CD4+ naïve T cells. (**i**) Within-person correlation matrices between cell subtypes for each mitochondrial feature over 9 weeks, illustrating to what extent cell subtypes are correlated with each other (co-regulation). (**j**) Average inter-correlation across all cell subtypes by mitochondrial feature (calculated using Fisher z-transformation) indicating the degree of coherence within person. (**k**) Comparison of co-regulation patterns among mitochondrial features between the cohort and the repeat participant. Each datapoint represents a cell subtype pair.

Figure 8

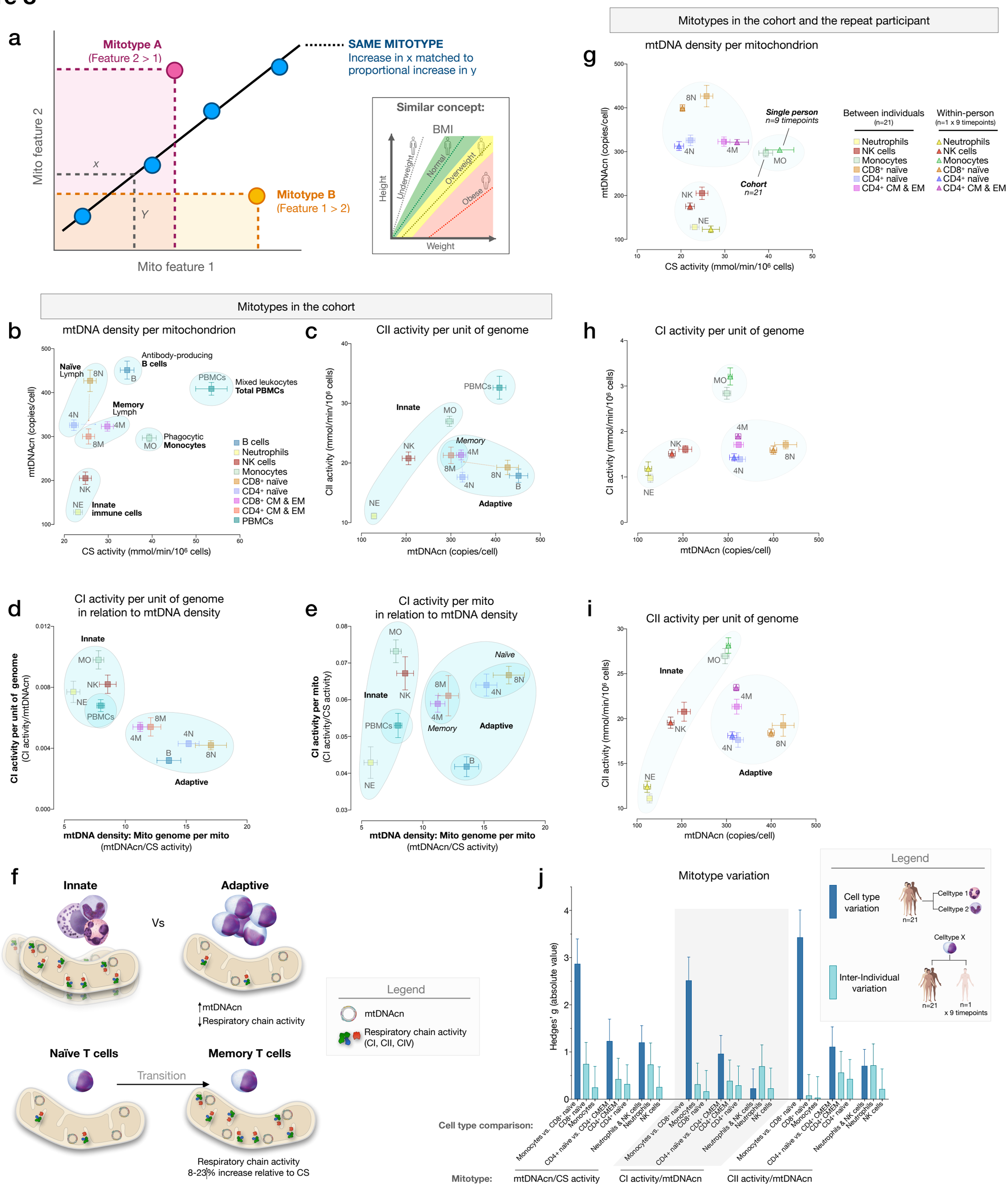

Figure 8 – Mitotypes in purified leukocyte populations from the cohort and repeated-measures.
(**a**) Schematic illustrating the multivariate approach to generate and visualize mitotypes by putting into relation two or more mitochondrial features. Notice the similarity and added insight relative to single metrics, similar to the integration of height and weight into body mass index (BMI). (**b-e**) Mitotypes plotted for each cell subtype among the cohort. Data are means and SEM. Overlaid shaded areas denote general leukocyte categories. (**f**) Summary of mitotype differences between (*i*) innate and adaptive subdivisions and (*ii*) naïve and memory T cells. (**g-i**) Validation of subtype-specific mitotype differences in the repeat participant, illustrating the conserved nature of mitotypes across individuals. Only the six cell subtypes analyzed in the repeat participant are plotted. (**j**) Comparison of the magnitude of the difference (Hedges' g) in mitotypes between cell types, and between individuals. Dark blue bars indicate the magnitude of the dominant difference in mitotypes between cell subtypes. Light blue bars indicate the magnitude of the difference in mitotypes between the cohort and the repeat participant within a cell type. Error bars reflect the 95% C.I. on the effect size.

Figure 9

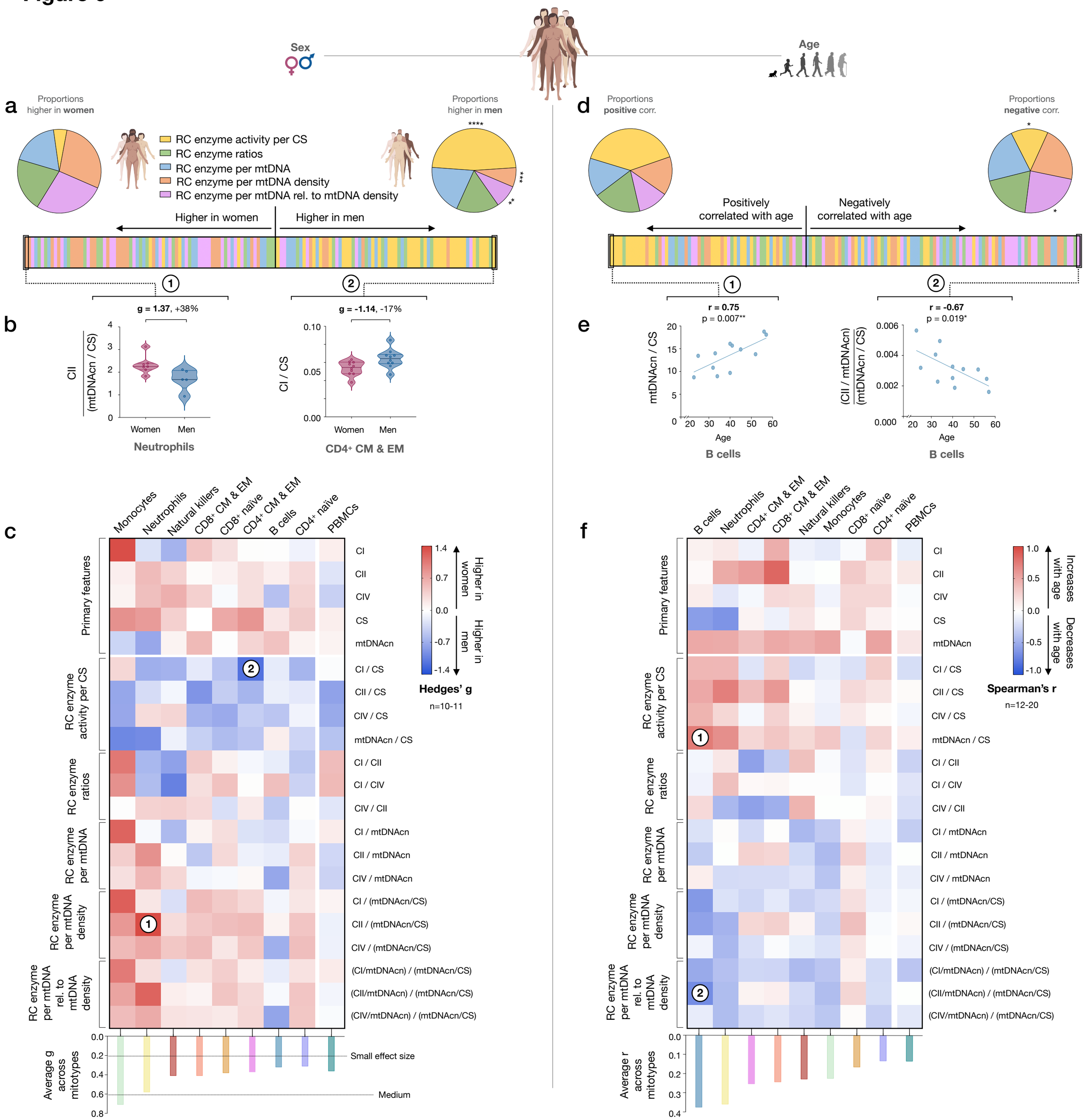

Figure 9 – Mitotype distribution and strength of difference across sex and age.

(**a**) Ranking of mitotype indices by their difference between women and men, quantified as the effect size (Hedges' g) between women and men. A total of 16 mitotype indices were generated, subdivided into 5 main color-coded categories (see Supplemental Figure 7). Pie charts illustrate the proportion mitotypes belonging to each category that are either higher in women (left) or in men (right). P-values for enrichment of sexually dimorphic mitotypes are derived from Chi-square test. (**b**) Violin plots illustrating the two mitotypes with the largest opposite sex differences, both showing large effect sizes (g). (**c**) Heatmap of sex differences (Hedges' g) for primary measures of mitochondrial function (top) and multivariate mitotypes (bottom) across cell subtypes. The histogram at the bottom shows the average absolute effect size across all mitotypes (calculated from absolute values). (**d**) Ranking of mitotype indices by the strength and direction of their association with age, with enrichment analysis analyzed as for sex (Chi-square test). (**e**) Spearman's r correlations of mitotypes/cell type combinations with the strongest positive and negative associations with age. (**f**) Heatmap of the age correlations (Spearman's r) for primary features and composite mitotypes across cell subtypes. The histogram at the bottom shows the average effect size (r) for each cell subtype (calculated using absolute values and Fisher z-transformation). p<0.05*, p<0.01**, p<0.001***, p<0.0001****.

Figure 10

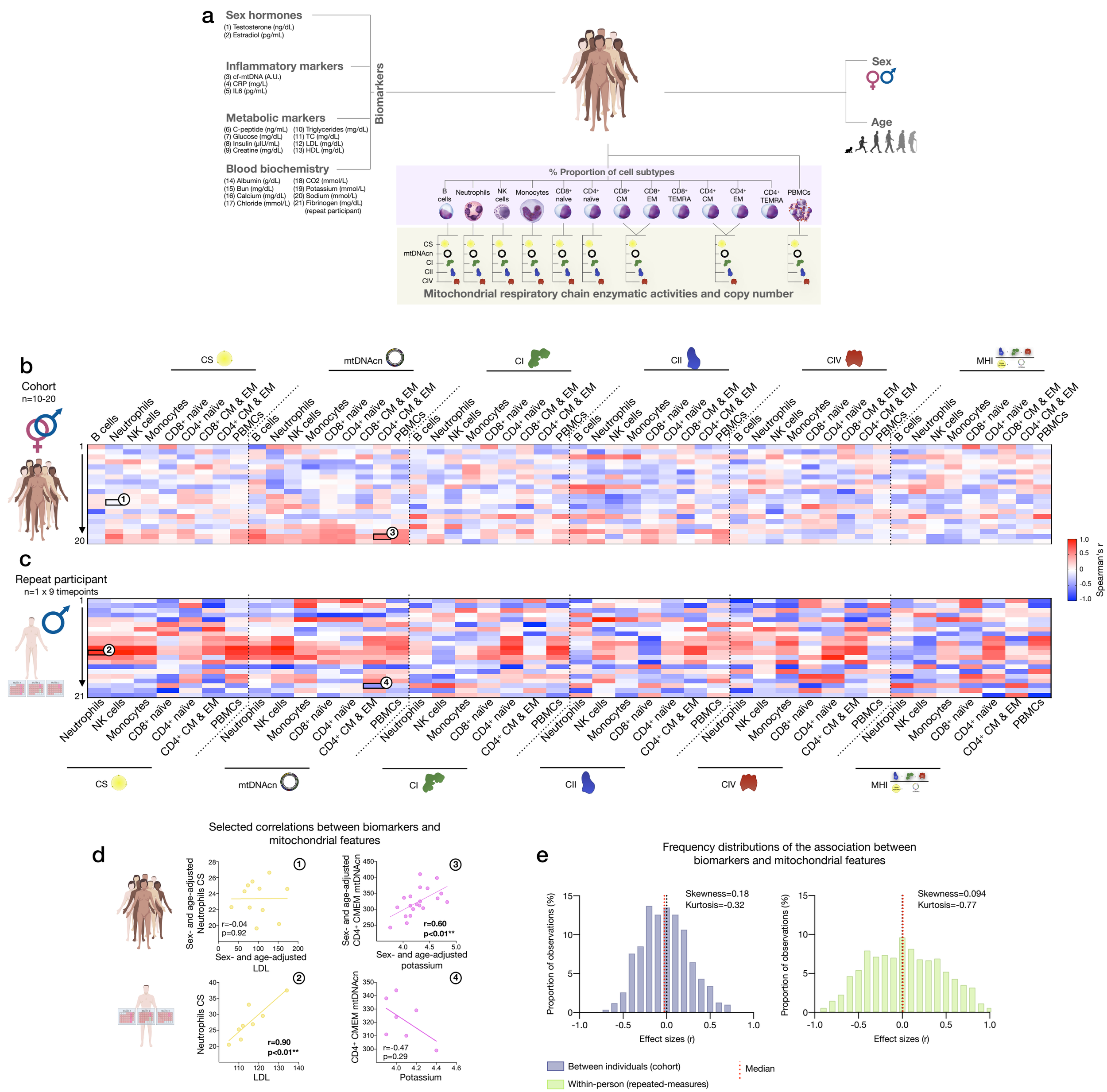

Figure 10 – Association of blood biomarkers with mitochondrial parameters across cell subtypes and primary mitochondrial features.
(**a**) Overview of blood biochemistry, hormonal, and metabolic biomarkers collected for each participant. (**b**) Sex- and age-adjusted correlations between blood biomarkers and mitochondrial features across cell subtypes for the cohort (n=10-20 per mito-biomarker combinations) shown as a heatmap. (**c**) Same as (b) but using repeated-measures of mitochondrial features and biomarkers in the repeat participant. (**d**) Scatterplots of the indicated correlations between Neutrophils CS activity and LDL cholesterol (left), and CD4+ CM-EM mtDNAcn and potassium (K^+) (right) for the cohort (top row) and the repeat participant (bottom row). (**e**) Frequency distributions of the aggregated effect sizes between biomarkers and mitochondrial features across cell subtypes for the cohort (total correlation pairs=1,080) and the repeat participant (total correlation pairs=882).